On the Understanding and Interpretation of Machine Learning Predictions in Clinical Gait Analysis Using Explainable Artificial Intelligence

Horst, F. [1,+,*]**, Slijepcevic, D.** [2,+,*]**, Lapuschkin, S.** [3]**, Raberger, A.-M.** [4]**,**

Zeppelzauer, M. [2]**, Samek, W.** [3]**, Breiteneder, C.** [5]**, Schöllhorn, W.I.** [1]

and Horsak, B. [4]

[1]*Department of Training and Movement Science, Institute of Sport Science, Johannes Gutenberg-University Mainz, Mainz, Germany*
[2]*Institute of Creative Media Technologies, Department of Media & Digital Technologies, St. Pölten University of Applied Sciences, St. Pölten, Austria*
[3]*Department of Video Coding & Analytics, Fraunhofer Heinrich Hertz Institute, Berlin, Germany*
[4]*Institute of Health Sciences, Department of Health Sciences, St. Pölten University of Applied Sciences, St. Pölten, Austria*
[5]*Institute of Visual Computing and Human-Centered Technology, TU Wien, Vienna, Austria*
[+]*These authors have contributed equally to this work.*

Correspondence*:
Fabian Horst: horst@uni-mainz.de
Djordje Slijepcevic: djordje.slijepcevic@fhstp.ac.at

ABSTRACT

Systems incorporating Artificial Intelligence (AI) and machine learning (ML) techniques are increasingly used to guide decision-making in the healthcare sector. While AI-based systems provide powerful and promising results with regard to their classification and prediction accuracy (*e.g.,* in differentiating between different disorders in human gait), most share a central limitation, namely their black-box character. Understanding which features classification models learn, whether they are meaningful and consequently whether their decisions are trustworthy is difficult and often impossible to comprehend. This severely hampers their applicability as decision-support systems in clinical practice. There is a strong need for AI-based systems to provide transparency and justification of predictions, which are necessary also for ethical and legal compliance. As a consequence, in recent years the field of *explainable AI* (XAI) has gained increasing importance. XAI focuses on the development of methods that enhance transparency and interpretability of complex ML models, such as Deep (Convolutional) Neural Networks. The primary aim of this article is to investigate whether XAI methods can enhance transparency, explainability and interpretability of predictions in automated clinical gait classification. We utilize a dataset comprising bilateral three-dimensional ground reaction force measurements from 132 patients with different lower-body gait disorders and 62 healthy controls. In our experiments,

we included several gait classification tasks, employed a representative set of classification methods, and a well-established XAI method – Layer-wise Relevance Propagation (LRP) – to explain decisions at the signal (input) level. The classification results are analyzed, compared and interpreted in terms of classification accuracy and relevance of input values for specific decisions. The decomposed input relevance information are evaluated from a statistical (using Statistical Parameter Mapping) and clinical (by an expert) viewpoint. There are three dimensions in our comparison: (i) different classification tasks, (ii) different classification methods, and (iii) data normalization. The presented approach exemplifies how XAI can be used to understand and interpret state-of-the-art ML models trained for gait classification tasks, and shows that the features that are considered relevant for machine learning models can be attributed to meaningful and clinically relevant biomechanical gait characteristics.

Keywords: explainable artificial intelligence, human gait classification, clinical gait analysis, layer-wise relevance propagation, statistical parameter mapping, ground reaction forces, convolutional neural networks

1 INTRODUCTION

Artificial Intelligence (AI) and machine learning (ML) techniques have become almost ubiquitous in our daily lives by supporting or guiding our decisions and providing recommendations. Impressively, there are certain tasks, such as playing complex board games like chess and Go, or classifying images, that AI has already been solving more efficiently and effectively than humans do (Cireşan et al., 2012; Esteva et al., 2017). It is not surprising that AI-based approaches are currently becoming increasingly popular in the healthcare sector (Topol, 2019). This trend has also been well recognized by the field of clinical gait analysis (CGA). CGA focuses on the quantitative description and analysis of human gait from a kinematic (*i.e.,* joint angles) and kinetic (*i.e.,* ground reaction forces and joint moments) point of view. Thereby, CGA produces a vast amount of data (Phinyomark et al., 2018; Halilaj et al., 2018), which are difficult to comprehend due to their multi-dimensional and multi-correlated nature (Chau, 2001; Wolf et al., 2006). In the last years, ML techniques and AI-based decision-support systems have been successfully employed to guide decision-making in CGA for various patient groups (Schöllhorn, 2004; Figueiredo et al., 2018) such as stroke (Lau et al., 2009), Parkinson's disease (Wahid et al., 2015), cerebral palsy (Van Gestel et al., 2011), multiple sclerosis (Alaqtash et al., 2011), osteoarthritis (Nüesch et al., 2012), and patients suffering from different functional gait disorders (Slijepcevic et al., 2017). While AI-based systems offer powerful and promising results in regard to classification accuracy and prediction, most share a central limitation, which is their black-box character (Adadi and Berrada, 2018). This means that even if the underlying mathematical principles in these systems are comprehensible, it is still very hard to understand if meaningful patterns and dependencies (*i.e.,* causalities) were learned and what the classification model has actually learned. In addition, the black-box character also hinders AI-based systems to provide justifications of their decisions. This is, however, necessary for compliance with legislation such as the General Data Protection Regulation (GDPR, EU 2016/679) (European Union, 2016; Adadi and Berrada, 2018; He et al., 2019). These factors currently limit the application of AI-based decision-support systems in medical practice (Holzinger et al., 2017; Samek et al., 2017).

Due to the aforementioned reasons, the field of *explainable Artificial Intelligence* (XAI) gained increasing attention in recent years. XAI aims to develop methods that improve the transparency, interpretability and explainability of complex ML models. The main goal is that (medical) professionals understand how and why a machine learning model resulted in a certain decision (Holzinger et al., 2019). Even though research

in XAI is still in an early stage, the application of such approaches to AI-based systems in medicine has already raised considerable interest (Holzinger et al., 2017; Tjoa and Guan, 2019).

Similar to other domains, a trade-off between classification accuracy and transparency of the classification models has to be made in the medical field. One reason is that potentially more accurate models, such as Deep Neural Networks (DNNs) are more complex and thus lack interpretability, whereas simpler models like decision trees exhibit a higher level of transparency but often achieve lower prediction accuracy (Turner, 2016). Consequently, simpler models have often been preferred for clinical applications in the past. Due to the recent success of XAI methods, the application of more complex classification models is currently gaining momentum in the clinical field.

Even though a variety of XAI methods are available for classification tasks (Section 2: Related work), their application to the field of CGA and motor rehabilitation has yet to be established. As Horst et al. (2019) demonstrated by distinguishing unique gait patterns of different individuals, the field of XAI offers great potential for future research and developments in CGA. Especially, the explanation of particular model decisions represents an indispensable form of transparency required by clinicians to build trust in AI-based systems (Tonekaboni et al., 2019). Therefore, the primary aim of this article is to investigate to which degree XAI can make automatic decisions more explainable in the context of CGA. We aim at introducing XAI to clinical gait classification by facilitating explainability and traceability of automatically derived decisions. In detail, this study exemplifies how XAI can be used to make clinical gait classification and prediction results understandable and traceable for clinical experts. For this purpose, we define different gait classification tasks, employ a representative set of classification methods, and a well-established XAI method – Layer-wise Relevance Propagation (LRP) – to explain decisions at the signal level.

Since there is no ground truth for automatically generated explanations in this context, we evaluate the quality of explanations from a clinical point of view by a clinical expert. In addition, as a second reference, we propose the use of Statistical Parameter Mapping (SPM) to verify the obtained results from a statistical point of view.

Our investigation follows three leading research directions:

- To what extent does a machine learning model for gait classification base its predictions on meaningful and clinically relevant biomechanical gait features?
- What is the role of data normalization and how does it affect machine learning-based gait classification and automatically generated prediction explanations?
- To what extent do XAI methods contribute to the improvement of transparency, understanding and interpretability of different classification methods?

To answer these questions we pursue an empirical approach. Based on a dataset containing ground reaction force measurements from clinical practice, we train classification models for different gait classification tasks and demonstrate the capabilities of XAI for the explanation of particular model decisions. Furthermore, we investigate their robustness to data normalization and incorporate a clinical expert to interpret and verify the results. The presented approach exemplifies how XAI can be used to better understand and interpret state-of-the-art machine learning models trained for gait classification tasks and shows that the features of gait patterns that are considered relevant for machine learning models can be attributed to meaningful and clinically relevant biomechanical gait characteristics.

2 RELATED WORK

Methods from XAI can be classified according to the type of explanation they provide. We distinguish between XAI approaches for (i) **data exploration**, (ii) **decision explanation** and (iii) **model explanation** based on an adaptation of the taxonomy introduced by Arya et al. (2019). In the following we briefly introduce the three different types of approaches and their capabilities.

Data exploration includes methods from the fields of visual analytics, statistics and unsupervised machine learning. As such, the methods are not capable of explaining a model but rather the data on which the model is trained. These methods focus on projecting the data into a space where it is possible to find meaningful structures or clusters and thus understand the data in more detail. A popular approach for data exploration introduced by Maaten and Hinton (2008) is T-distributed Stochastic Neighbor Embedding (t-SNE), which projects high-dimensional data into a lower-dimensional and visualizable space. The projection is performed in a way that the cluster structure in the original data space is optimally exposed. Thereby, an understanding of the data and the identification of typical patterns and clusters in the data is facilitated. Other approaches in this category are visual analytics approaches that employ advanced techniques for the interactive visualization of data to support data exploration, *i.e.,* finding characteristic patterns or dependencies within data (Wagner et al., 2019; Wilhelm et al., 2015).

Decision explanation aims at providing an explanation for the local behavior of a model, *i.e.,* the prediction for a given input instance. For a classification task, these methods can provide, for example, explanations about which part of the input influenced the classifier's decision most. For classification of gait data, the explanation should highlight all relevant signal regions and characteristic signal shapes in the input data, which are associated with a particular gait disorder. Two main categories can be distinguished for explaining the local behavior of a machine learning model: i) *self-explaining* models and ii) *post-hoc* methods.

Self-explaining models consist of components that learn relationships between input data and predictions during training. Simultaneously, they learn how these relationships relate to terms from a predefined dictionary and consequently generate explanations from them. A self-explaining approach which does not visually highlight relevant regions in input data but generates textual explanations was proposed by Hendricks et al. (2016). This self-explaining model combines a Convolutional Neuronal Network (CNN) and a Recurrent Neuronal Network (RNN). The CNN learns discriminative features to perform a classification task, while the RNN generates textual explanations of the prediction. This approach cannot be applied to a previously trained model in a post-hoc manner. This limits the practical applicability of such approaches.

Post-hoc models provide much greater applicability as they can be applied to already trained models. Post-hoc methods can be further sub-divided into i) propagation-based, ii) perturbation-based, and iii) Shapley-value-based methods.

Propagation-based methods determine the contributions of each input feature by (back-)propagating some quantity of interest from the model's output layer to the input layer. Sensitivity Analysis (Zurada et al., 1994) has been introduced to Support Vector Machines (SVM) (Baehrens et al., 2010) and CNNs (Simonyan et al., 2013) in form of saliency maps. Layer-wise Relevance Propagation (LRP) (Bach et al., 2015; Montavon et al., 2019) and Deep Learning Important FeaTures (DeepLIFT) (Shrikumar et al., 2017) are methods that propagate importance scores from the output layer back to the input, thereby enabling the identification of positive and negative evidences for a specific prediction. Sensitivity Analysis and the therewith obtained explanations in general suffer from the effects of shattered gradients (Balduzzi et al.,

2017), especially so in more complex (deeper) networks. Modern approaches to DNN interpretability such as LRP or DeepLift do not have this problem and work well for a wider range of network architectures, and models in general (Montavon et al., 2018; Kohlbrenner et al., 2019).

Perturbation-based methods, such as those introduced by Fong and Vedaldi (2017) or Zintgraf et al. (2017), treat the model as a black box and are applied to pairs of occluded input and the respective output values. While some methods produce explanations directly from a perturbation process, others employ a learning component – *e.g.,* the Interpretable Model-agnostic Explanations (LIME) method (Ribeiro et al., 2016) – to estimate locally interpretable surrogate models mimicking the decision process of the black-box model. Perturbation-based methods can be considered to be model-agnostic, as they do not require access to internal model parameters or structures to operate. However, this model-agnosticism is bought at a considerable computational cost, compared to propagation-based approaches.

Shapley-value-based methods attempt to approximate the Shapley values of a given prediction. For this purpose, the effect of omitting an input feature is examined, taking into account all possible combinations of other input features, that can be included or excluded (Štrumbelj and Kononenko, 2014). Lundberg and Lee (2017) proposed the SHapley Additive exPlanations (SHAP) method, which is a unified approach building upon the theory of Shapley values and existing propagation-based and perturbation-based methods, *e.g.,* LIME, DeepLIFT, and LRP.

Model explanation provides an interpretation of what a trained model has learned, *i.e.,* the most characteristic representations or prototypes for an entire class are visualized (*e.g.,* a class of gait disorders in CGA). These methods can indicate which classes overlap and point out ambiguous input features. In addition to saliency maps, Simonyan et al. (2013) proposed a method for generating a representative visualization for a specific class that was learned by a CNN. For this purpose, they applied activation maximization, *i.e.,* starting with a blank image, each pixel is changed by means of backpropagation so that the activity of a neuron is increased. The resulting visualizations give a first impression about the patterns learned but are highly abstract and can only be interpreted to a limited extent. To generate visualizations that are easier to interpret, Nguyen et al. (2016) proposed a method to constrain the optimization process by image priors that were learned automatically. Lapuschkin et al. (2019) proposed the Spectral Relevance Analysis (SpRAy) which summarizes a model's learned strategies by analyzing similarities and dissimilarities over large quantities of input relevance maps computed with respect to a category of interest.

3 METHODS

3.1 Data Recording and Dataset

For the gait classification task we utilized a subset of a large-scale dataset which is currently prepared for publication in an open-source online repository as the GAITREC dataset (reference to the dataset will be made public upon publication). This dataset is part of an existing clinical gait database maintained by a local Austrian rehabilitation center. Prior to all of our experiments approval was obtained from the local Ethics Committee (#GS1-EK-4/299-2014). The employed dataset contains bilateral three-dimensional ground reaction force (GRF) recordings of patients and healthy controls walking unassisted at self-selected walking speed on an approximately 10 m walkway with two centrally-embedded force plates (Kistler, Type 9281B12, Winterthur, CH). Data were recorded at 2000 Hz, filtered with a zero-lag Butterworth filter of 2nd order with a cut-off frequency of 20 Hz, time-normalized to 101 points (100% stance), and amplitude-normalized to 100% body weight. During one session subjects walked barefoot or in socks

until a minimum number of 5 valid recordings were available. Recordings were defined as valid by an experienced assessor.

In total, the dataset comprises GRF measurements from 132 patients with lower-body gait disorders (GD) and data from 62 healthy controls (HC), both of various physical composition and gender. The dataset includes three classes of orthopaedic gait disorders associated with the hip (H, N=37), knee (K, N=52), and ankle (A, N=43). For class-specific demographic details of the data refer to Table 1. The dataset is balanced regarding the number of recorded sessions per person and the number of trials per person. Figure 1 shows an overview of all GRF measurements of the affected side (except for healthy controls where each step is visualized) per class and the associated mean and standard deviation. The GD classes (A, H, and K) include patients after joint replacement surgery, fractures, ligament ruptures, and related disorders associated with the above-mentioned anatomical areas. A well-experienced physical therapist with more than a decade of clinical experience manually labeled the dataset based on the available medical diagnosis of each patient.
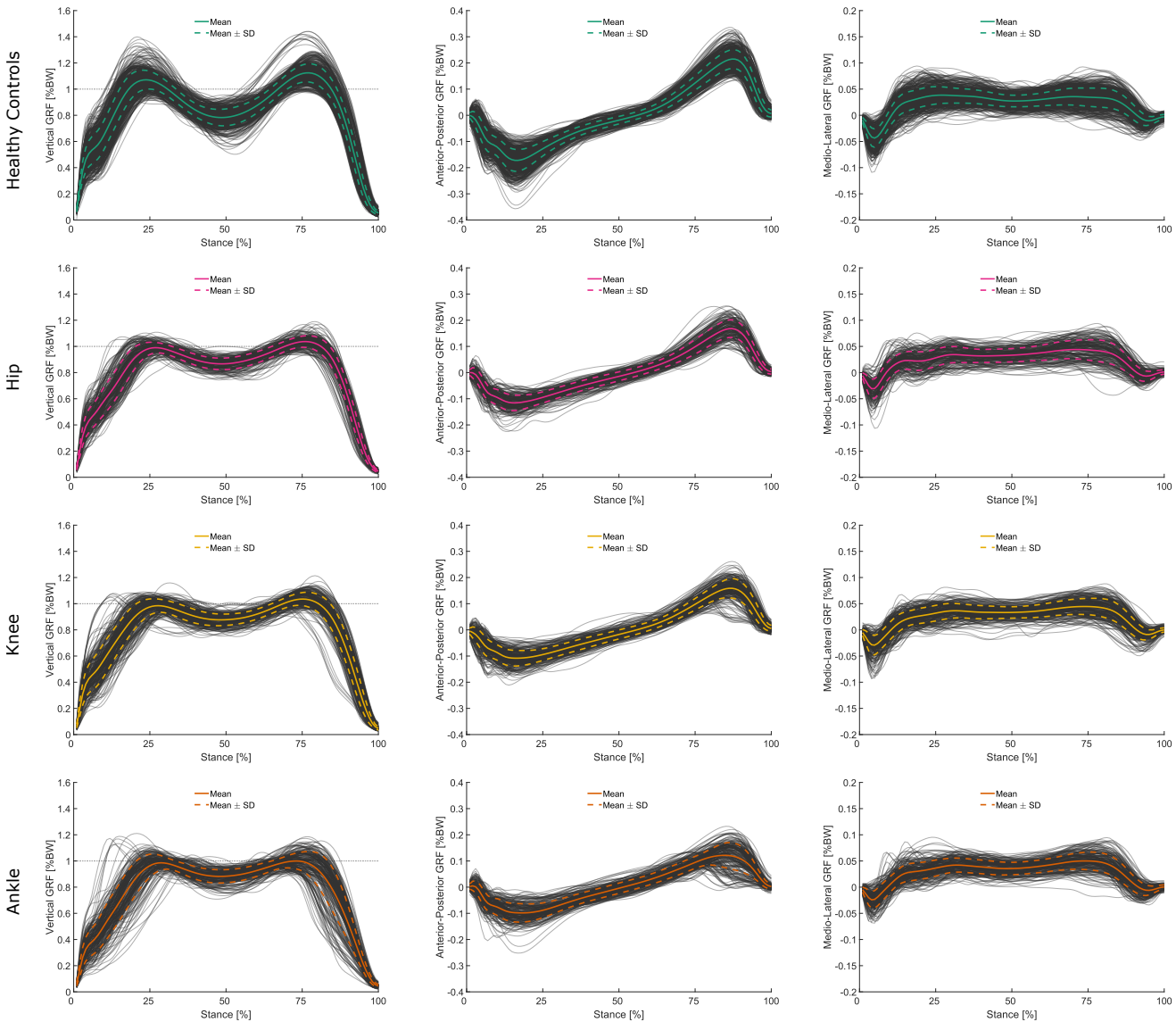
Table 1. Demographic details of the employed dataset for each pre-defined class.

Classes	N	Age (yrs.) Mean (SD)	Body Mass (kg) Mean (SD)	Sex (m/f)	Num. Trials
Healthy Control	62	36.0 (10.8)	72.3 (15.0)	28/34	310
Hip	37	44.2 (12.5)	81.4 (14.1)	31/6	185
Knee	52	43.5 (13.8)	85.6 (16.4)	37/15	260
Ankle	43	42.6 (10.9)	91.6 (20.4)	36/7	215
Total	**194**	**41.1 (12.4)**	**81.9 (18.0)**	**132/62**	**970**

3.2 Decision Explanation

As proposed by Bach et al. (2015), we employed Layer-wise Relevance Propagation (LRP) as a method for decision explanation. LRP decomposes the prediction $f(x)$ of a learned function f given an input vector x into time- and channel-resolved input relevance values R_i for each discrete input unit x_i. This enables to explain the prediction of a machine learning model as partial contributions of an individual input value (see Figure 2 for an overview of the approach). LRP indicates which information a model uses to predict in favor or against an output class. Thereby, it enables the interpretation of input relevance values and their dynamics as representation for a certain class (*i.e.,* healthy controls or functional disorders in ankle, knee or hip). Given that the models investigated in this study are comparatively shallow and are largely unaffected by detrimental effects such as gradient shattering (Balduzzi et al., 2017; Montavon et al., 2019), we performed relevance decompositions according to LRP$_\varepsilon$ with $\varepsilon = 10^{-5}$ in all layers across the different model architectures (Kohlbrenner et al., 2019).
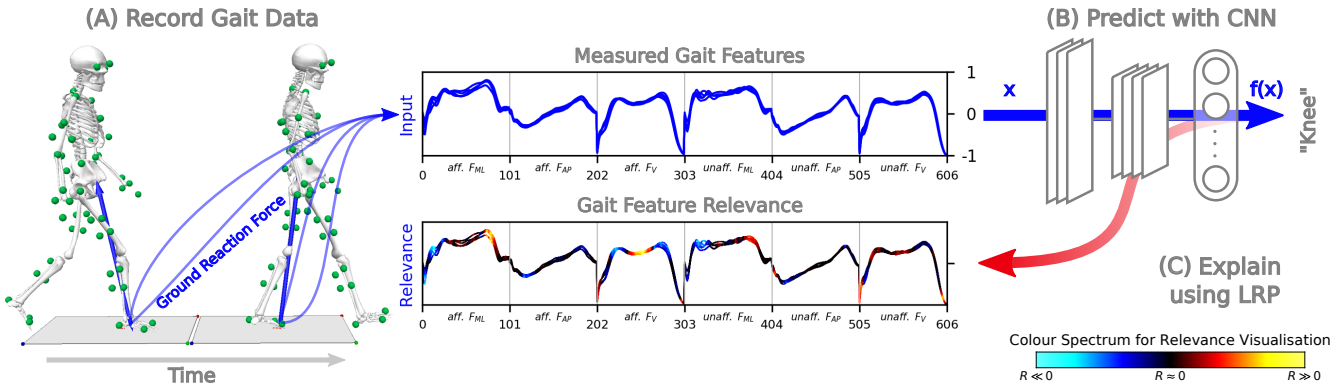
Another approach which recently faced increased attention in the gait analysis community is the application of Statistical Parameter Mapping (SPM). While standard inference statistical approaches tend to reduce time-continuous signals to single time-discrete values for statistical testing, SPM allows to use the entire 1D time-continuous signals to make probabilistic conclusions based on the random behavior of a 1D observational unit. It follows the same notion and logic as classical inference statistics. The main advantages of SPM are that the statistical results are presented in the original sampling space and that there is no need for a (potentially biasing) parameterization technique (Pataky, 2012, 2010). Therefore, SPM can serve as a valuable and statistically-based verification method in the context of XAI in clinical

Figure 1. Visualization of vertical (left panel), anterior-posterior (central panel), and medio-lateral (right panel) force components of the body weight-normalized GRF measurements of the affected side available per subject and class. For healthy controls all available measurements are visualized. Mean and standard deviation signals (calculated per class) are highlighted as solid and dashed colored lines.

biomechanics. We used independent *t*-tests from the SPM1D[1] package provided by Pataky (2012) for Matlab to investigate differences between the concatenated GRF signals between each class. The alpha level was set a priori to 0.05. The output of SPM provides *t*-values for each point of the investigated time series and the threshold corresponding to the chosen alpha level. The *t*-values exceeding this threshold (marked as gray-shaded areas in our results in Figures 4, 5, and 6) indicate statistically significant differences in the corresponding sections of the time series. Additionally, we computed the effect size by transforming the resulting *t*-values to Pearson's correlation coefficient *r* using the definition by Rosenthal (1986).

---

[1] SPM1D v.0.4, http://www.spm1d.org/

Figure 2. Exemplary overview of our proposed workflow for data acquisition, prediction and decision explanation in automated gait classification, showing the data of subject 46 belonging to the knee disorder class. (A) The clinical gait analysis consists of five recordings of each subject walking barefoot (unassisted) a distance of 10 m at a self-selected walking speed. Two centrally-embedded force plates capture the three-dimensional ground reaction forces (GRFs) during the stance phase of the right and left foot. (B) The GRF comprising the medio-lateral (F_{ML}), anterior-posterior (F_{AP}), and vertical (F_V) force components of the affected and unaffected side are used as time-normalized and concatenated input vector x (1×606-dimensional) for the prediction of the knee disorder class using a classifier (*e.g.,* CNN). (C) Decomposition of input relevance values using LRP. The color spectrum for the visualization of input relevance values of the model predictions is shown in the bottom right corner. Black line segments are irrelevant to the model's prediction. Warm hues identify input segments causing a prediction corresponding to the class label, while cool hues are features contradicting the class label.

In this context, we do not expect LRP and SPM to produce identical results as they assess the data from different perspectives, but they should reveal similar trends as we assume that discriminatory information learned by a classifier should also be statistically significant.

3.3 Experimental Setup

The following classification tasks represent the basis of our investigation:

- binary classification between healthy controls and all gait disorders (HC/GD),
- binary classification between healthy controls and each gait disorder separately (*i.e., HC/H, HC/K,* and HC/A),
- multi-class classification between healthy controls and each gait disorder separately ($HC/H/K/A$),
- and multi-class classification between each gait disorder separately ($H/K/A$).

The six classification tasks are based on a concatenated input vector of the three-dimensional GRF signals from both force plates and resulted in 1×606-dimensional input vectors per gait trial. The three-dimensional GRF signals are the medio-lateral shear force (F_{ML}), anterior-posterior shear force (F_{AP}), and vertical force (F_V). The dataset included only unilateral gait disorders and the data of the affected side (input features: 1 to 303) was concatenated before the data of the unaffected side (input features: 304 to 606) in the input vector. For the healthy controls the order was randomly assigned, while ensuring an equal distribution, in order to avoid any bias regarding the side (as there is no affected and unaffected side in the data of this class).

Normalization of input vectors is commonly applied to ensure an equal contribution of all six GRF signals to the classification models and thus avoids that signals with larger numeric ranges dominate those with smaller numeric ranges (Hsu et al., 2016; Chollet, 2017). In order to evaluate the robustness of our

models' predictions and input relevance estimates with respect to normalization, we firstly conducted experiments without normalization. In a second step, we conducted the same experiments applying a min-max normalization and thereby scaled each signal to the range $[-1, 1]$. The global minimum and maximum values were determined separately for each GRF signal and over all trials. Although feature extraction is an established step in the (gait) classification pipeline (Halilaj et al., 2018; Slijepcevic et al., 2018), the improved applicability and interpretation of the XAI methods have led us to refrain from using methods such as Principle Component Analysis (PCA) in the present work.

In our experiments, three representative machine learning approaches, *i.e.,* (linear) Support Vector Machine (SVM), Multi-layer Perceptron (MLP), and Convolutional Neural Network (CNN) were compared in terms of prediction accuracy and learned input relevance patterns. The SVM models were trained using a standard quadratic optimization algorithm, with an error penalty parameter $C = 0.1$ and ℓ_2-constrained regularization of the learned weight vector w. The MLP models comprised of three consecutive fully connected layers with ReLU non-linearities activating the hidden neurons and a final SoftMax activation in the output layer. The size of both hidden layers is 768 whereas the size of the output layer is c, where c is the number of target classes. The CNN models process the given data via three consecutive convolutional layers, with a *<filter size>-<stride>-<output channel>* configuration of 8-2-24, 8-2-24 and 6-3-48, and ReLUs for non-linear neuron activation. The resulting 48×48 feature mapping is then unrolled into a 2304-dimensional vector, and fed into a fully connected layer. This fully connected layer is topped with a SoftMax output activation, which is acting as an multi-class predictor output towards the c target classes. Both, the MLP and CNN models, have been trained via standard error back-propagation using stochastic gradient descent (LeCun et al., 2012) and a mean absolute (ℓ_1) loss function. The training procedure was executed for $3 \cdot 10^4$ iterations of mini batches of five randomly selected training samples and an initial learning rate of $5 \cdot 10^{-3}$. The learning rate was gradually decreased after every 10^4-th training iteration to 10^{-3} by a factor of 0.2 and then to $5 \cdot 10^{-4}$ by a factor of 0.5. Model weights were initialized with random values drawn from a normal distribution with $\mu = 0$ and $\sigma = m^{-\frac{1}{2}}$, where m is the number of inputs to each output neuron of the layer (LeCun et al., 2012). Since the CNN receives as input a 1×606-dimensional input vector, its convolution operations can be understood as 1D convolutions, moving over the time axis only. We used 1D convolutions to maintain comparability with the two other classification methods (MLP and SVM). However, preliminary experiments demonstrated negligible differences between 1D and 2D CNNs.

The prediction accuracies were reported over a stratified ten-fold cross-validation configuration, where eight parts of the data are used for training, one part is used as validation set and the remaining part is reserved for testing. The samples from each class were distributed evenly while ensuring that all gait trials from an individual subject are placed in the same partition of the data to rule out subject-related information influencing the measured model performance during testing. All results are reported as mean with standard deviation (SD), unless otherwise stated. Additionally, we calculated the Zero Rule baseline (ZRB) for each classification task. The ZRB refers to the theoretical accuracy obtained by assigning class labels according to the prior probabilities of the classes, *i.e.,* the target labels are always set to the class with the greatest cardinality in the training dataset.

With respect to the decision explanations for a specific classification task, we decomposed the input relevance values of each gait trial with LRP. This was possible because each trial was tested exactly once within the cross-validation configuration described above. For the purpose of our analysis, however, we used LRP only to decompose the prediction value corresponding to the class label of the trial. Thus, for the

visualizations, we averaged the underlying GRF signals as well as the resulting input relevance values over all trials of the corresponding class within a given classification task.

The data analysis was conducted within the software frameworks of Matlab 2017b (MathWorks, USA) and Python 3.7 (Python Software Foundation, USA).

4 RESULTS
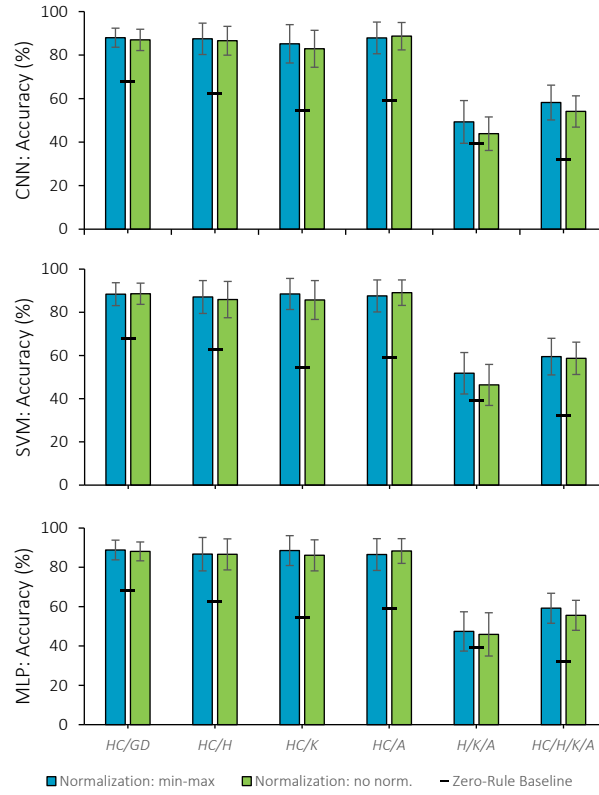
The mean prediction accuracy showed a clear superiority over the ZRB for all three classification methods (CNN, SVM, and MLP) and all classification tasks except for task $H/K/A$ (see Figure 3).

A 2×2 repeated measures analysis of variance (ANOVA) (classification method: CNN, SVM, and MLP; normalization: min-max and no normalization) conducted for each classification task indicated a significant difference in classification accuracy between the three classifiers for tasks HC/GD ($F_{2,18} = 3.949$, p = 0.038, $\eta_p^2 = 0.305$), HC/K ($F_{2,18} = 16.803$, p < 0.001, $\eta_p^2 = 0.651$), and $HC/H/K/A$ ($F_{2,18} = 3.718$, p = 0.045, $\eta_p^2 = 0.292$). Additional pairwise and Bonferroni-corrected post-hoc tests revealed that the CNN resulted in a marginally (~1%), but significantly (p = 0.046) lower accuracy than the MLP for task HC/GD, and that the accuracy of the CNN was significantly (p < 0.04) lower compared to both other classifiers in task HC/K (~3%). No other differences were found for the classifiers' performances. Regarding the normalization, only for task $HC/H/K/A$ ($F_{1,9} = 5.281$, p = 0.047, $\eta_p^2 = 0.370$) the ANOVA indicated that the accuracy was overall ~2.8% higher with normalization than without. For other tasks no other effects and differences were indicated.

As an example for decision explanation using LRP, Figure 4 shows the averaged signals together with the color-coded averaged relevance values for each of the 606 input values for task HC/GD with non-normalized GRF signals. The input relevance values point out which GRF characteristics were most relevant for (or contradictory to) the classification of a certain class (HC or GD). For visualization, input values neutral to the prediction ($R_i \approx 0$) are shown in black color, while warm hues indicate input values supporting the prediction ($R_i \gg 0$) of the analyzed class and cool hues identify contradictory input values ($R_i \ll 0$). For binary classification tasks (HC/GD, HC/H, HC/H, HC/K, and HC/A), note that a high input relevance value for one class results in a contradictory input relevance value for the other class. Therefore, the total relevance is a good indicator for the overall relevance of an input value for a respective classification task.

The highest input relevance values were observed in F_V of the affected side, as illustrated in Figure 4. In the same way, the mean GRF signals of both classes (see Figure 4A) as well as the SPM analysis (gray-shaded areas in Figure 4) highlighted statistically significant differences between both classes in the same regions of F_V of the affected side. While LRP points out that the input values of both horizontal shear forces (F_{AP} and F_{ML}) appear to be mostly neutral to the prediction, it is noticeable that the SPM analysis highlighted a lot more regions within F_{AP} and F_{ML} as statistically significantly different between the two classes. This contradictory behavior is subject to further analysis below.

In a second experiment, the classification of (HC/GD) based on min-max normalized GRF signals confirmed the identified regions of high relevance in F_V observed in Figure 4, but additionally highlighted regions of high relevance in both horizontal shear forces (see Figure 5). The input relevance values highlight that the regions with the highest input relevance values for the prediction can be observed at approximately 20% of the stance phase in F_{AP} of the unaffected side, at approximately 80% of the stance phase in F_{AP} of the affected side and the F_V throughout the stance phase from approximately 20% till 80% of the stance
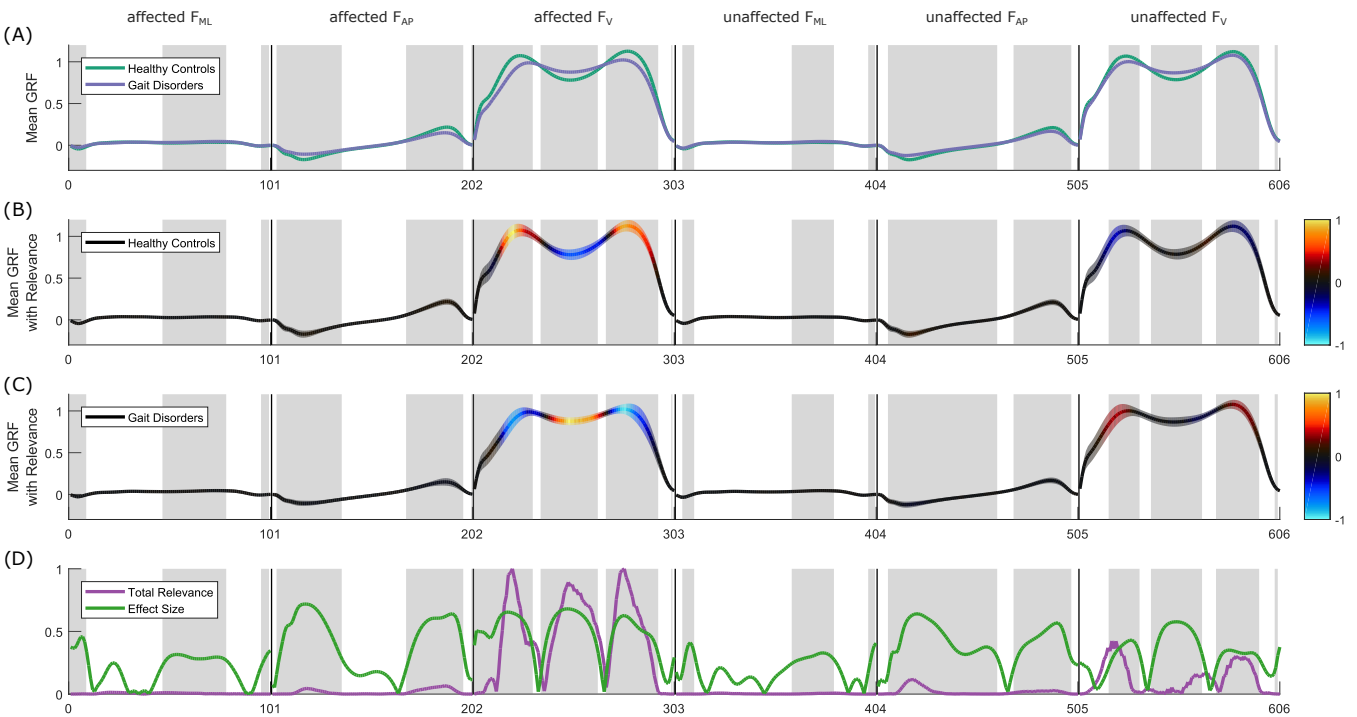
Figure 3. Overview of the prediction accuracy obtained for the three employed classification methods (CNN, SVM and MLP) and all six classification tasks with min-max normalized and non-normalized input signals, reported in pairs of mean (standard deviation) over the ten-fold cross validation in percent.

phase. In addition, high input relevance values can be observed in the F_V during the initial and terminal contact of the affected and unaffected side.

Decision explanation methods like LRP further allow to compare and better understand different classification methods. Figure 6 shows the results for all three employed classification methods (CNN, SVM, and MLP) and confirms general comparability between these for the task HC/GD (with min-max normalized GRF signals as in Figure 5). However, with respect to F_V the highest input relevance values can be observed in the peak regions for the CNN, while the highest input relevance values for SVM and MLP are present during the initial and terminal contact.

5 DISCUSSION
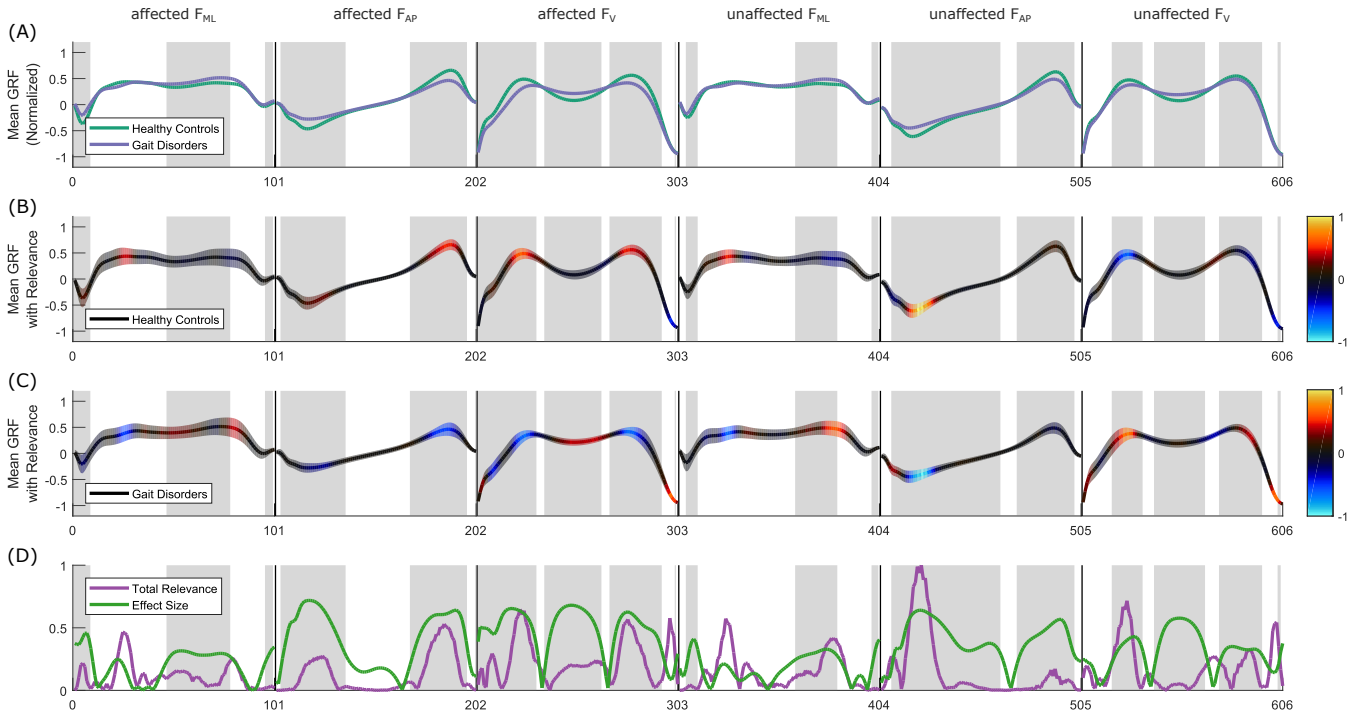
The primary aim of this article is to investigate whether XAI methods can enhance transparency, explainability and interpretability of predictions in automated clinical gait classification. There are three dimensions in our experimental setup: (i) different classification tasks, (ii) different classification methods, and (iii) data normalization. The classification results are analyzed, compared and interpreted in terms of classification accuracy and relevance of input values for specific decisions. These input relevance information is, furthermore, evaluated and compared from a statistical and clinical viewpoint.
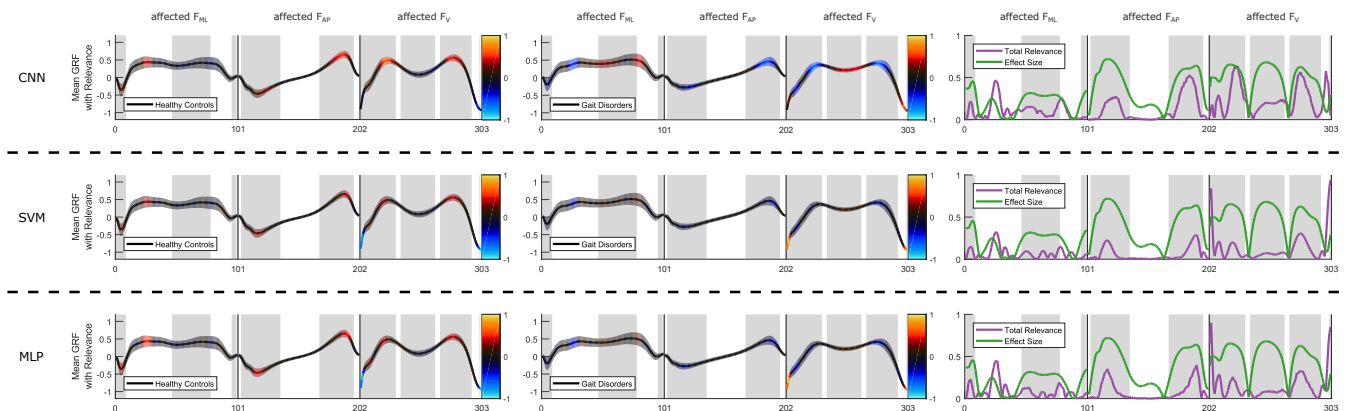
Figure 4. Results overview for the classification of healthy controls (HC) and the aggregated class of all three gait disorders (GD) based on non-normalized GRF signals using a CNN as classifier. (A) Averaged GRF signals for HC and GD. The first three signals represent the three GRF components of the affected side and are followed by the three GRF components of the unaffected side. Note that the data for both sides is composed of three GRF components (*e.g.,* input features of the affected side: 1 to 101 (F_{ML}), 102 to 202 (F_{AP}), and 203 to 303 (F_V)). This means, for example, that input features 21 (F_{ML}), 122 (F_{AP}) and 233 (F_V) all correspond to the relative time of 20% of the same stance phase. The shaded areas highlight areas in the input signals where SPM resulted in a statistically significant difference between both classes (*i.e., HC* and GD). (B) Averaged GRF signals of all test trials as a line plot for the healthy controls class, with a band of one standard deviation, color coded via input relevance values for the class (HC) obtained using LRP. (C) Averaged GRF signals of all test trials as a line plot for the class of all the gait disorders (GD), in the same format as in (B). (D) Line plot showing the effect size obtained from SPM and total relevance based on the absolute sum of the input relevance values of both classes (HC and GD). The total relevance indicates the common relevance of the input signal for the classification task.

5.1 Classification Results

The results expressed in terms of classification accuracy (presented in Figure 3) demonstrate a comparable level of performance between the three different machine learning methods (CNN, SVM, and MLP). An objective analysis of the explainability is only meaningful if a classifier robustly differentiates between the target classes. Therefore, we excluded the tasks $HC/H/K/A$ and $H/K/A$ from our further investigation. The inability to distinguish the classes in both multi-class classification tasks indicate that gait disorders exhibit complex compensation across several joints, which are difficult to fathom in detail by a measure such as the GRF. Therefore, the tasks $HC/H/K/A$ and $H/K/A$ bear the potential risk that no robust and stable patterns can be found and influence of noise and spurious correlations biases the explainability analysis. For the binary classification tasks this risk is much lower, because the higher classification accuracies obtained (and deviations from the Zero Rule baseline) suggest that robust features can be found in the input data.

Figure 5. Same experiment as shown in Figure 4 but using min-max normalized GRF signals.


Figure 6. Comparison of different methods (CNN, SVM, and MLP) for the classification of healthy controls and the class of all three gait disorders (HC/GD) based on min-max normalized GRF signals (only the signals of the affected side are shown). The comparison is based on the decomposed input relevance values for both classes (HC and GD), their total relevance determined by LRP as well as statistically significant differences (gray-shaded areas) and effect sizes obtained by SPM. Note that the effect size (green curve) is the same for all three classifiers but the total relevance varies.

Another aspect we assessed is the influence of normalization on the input data (see Figure 3). The normalization of the input data is important for machine learning, since highly differing value ranges can have a negative influence on the classifier, *e.g.,* input variables with a higher value range have a stronger influence on the decision (Hsu et al., 2016; Chollet, 2017). In addition, non-normalized data can lead to unstable and non-convergent learning. A comparison between the amplitude value ranges of the non-normalized shear forces (F_{AP} and F_{ML}) and F_V clearly showed a significant difference (see Figure 4). Therefore, we min-max normalized the data to investigate the degree of influence of normalization on the classification results and the derived explanations.

Surprisingly, min-max normalization does not significantly improve the classification results (see Figure 3) for all investigated binary classification tasks (HC/GD, HC/H, HC/K, and HC/A). The absence of an increase in prediction accuracy raises the question whether the use of F_V is already sufficient for the given classification tasks. Although normalization does not improve the classification accuracies, the explainability results are strongly affected. We discuss this divergent behavior in the following.

5.2 Explainability Results

In the following, we discuss the explainability results using the detailed example of the CNN as a classifier and HC/GD as a classification task. Compared to this modality, we also summarize relevant differences in the results for other classifiers and classification tasks in this section. The visualizations for all classification tasks and classification methods can be found in the supplementary material (see Supplementary Figures S 1–S 24).

Which features are most relevant? For the classification of non-normalized GRF signals with a CNN (see Figure 4), the most relevant input values are mainly located in F_V of the affected side, *i.e.,* especially the two peaks and the valley in between are relevant for the decision. This shows that the CNN learned that classes HC and GD differ most in these three sections of the signals. These results were also confirmed in our earlier studies, *e.g.,* where the examination of the most frequently used discrete parameters has also shown high relevance for the peaks of F_V and the valley in between (Slijepcevic et al., 2017).

Is the unaffected side important? Identified relevant regions are considerably less pronounced in F_V of the unaffected side, but they correlate to a large extent with those of the affected side, except that only the rear part of the valley and not the entire valley is relevant (best recognized from the total relevance curve in Figure 4D). In earlier studies (Slijepcevic et al., 2018, 2019), we showed that the omission of the unaffected side during classification negatively affected classification accuracy. The explainability results confirm this observation. Thus, the unaffected side seems to capture complementary information relevant to the classification task.

Are the shear forces relevant for the task? A minimal degree of relevance can also be observed in the peaks of the affected and unaffected F_{AP} signals. The absence of evident relevant regions from the shear forces (F_{AP} and F_{ML}) does not confirm our results from previous studies where we showed that adding shear forces indeed improved classification performance (leading even to peak performance). From this experiment, the question whether or not shear forces are beneficial for the task cannot be answered conclusively. Interestingly, the statistical analysis via SPM highlights regions in the shear forces that differ statistically significantly between classes HC and GD.

What is the impact of normalization on explainability? The reason for the absence of relevant regions in the shear forces could be their small value range. The rather small value range compared to the F_V component may have negligible influence on the training process of the classifiers. We applied normalization to the inputs to answer this question. The results for the same classification task and CNN architecture with min-max normalized input data show that with normalization numerous relevant regions can be found in the shear forces of the affected and unaffected side (see Figure 5). Normalization amplifies the relevance of values in the shear forces and thereby makes them comparably important as F_V. Thus, normalization is important to obtain unbiased explainability results.

Are all identified relevant regions necessary for the task? In general, with min-max normalized input, many regions of the GRF signals appear relevant for the classification of a particular class. The classification performance with and without normalization does, however, not vary significantly (see Figure 3). This

raises the question whether all identified regions are actually necessary to achieve peak performance in classification or whether some of them are redundant. Note that the assumption of redundancy is supported by the fact that the three force components represent individual dimensions of the same three-dimensional physical process. Thus, strong correlation in the data is a priori given. To answer this question we occluded parts of the input vector in the classification experiment and evaluated the changes in classification performance. Occlusion is realized by replacing the shear forces (F_{AP} and F_{ML}) of both sides with zero values and retraining the classifier. Table 2 shows the classification results for the occluded input. To enable easier comparison with the previous results, the deviation from the mean classification accuracy of the non-occluded experiments (from Figure 3) are displayed for all binary classification tasks. In general, the results decrease on average when the shear forces are occluded, except for task HC/A with min-max normalized input data. Furthermore, the decrease is more pronounced for min-max normalized input data than for non-normalized input data. This further corroborates our assumption that normalization is important to take information from shear forces into account. However, the classification results of the binary classification tasks are not statistically significantly influenced by the occlusion of shear forces. This was also confirmed by several dependent t-tests (p > 0.05). Our results indicate that the relevant regions identified by LRP may represent an over-complete set which exhibits a certain degree of redundancy. Removing one section does not necessarily reduce classification performance. However, model predictions that are based on a higher number of features have been shown to be more robust to noise and possibly also outliers and missing data (Horst et al., 2019).

Are shear forces relevant for the task (question revisited)? The effects of occluded shear forces are illustrated in Table 2. Especially for experiments with min-max normalized data, this lead to a decrease in performance (*e.g.,* HC/H and HC/K). Thus, the relevant regions in the shear forces cannot be completely redundant to those in F_V and, therefore, represent also complementary information. This is also in line with our previous quantitative evaluations (Slijepcevic et al., 2019).

Table 2. Classification results for the experiment with occluded shear forces (F_{AP}, F_{ML}), in percent. The results are reported as mean deviation from the classification rates of the original input vector presented in Figure 3, *i.e.,* negative values signify a decrease and positive values an improvement in accuracy. Note that the Zero Rule baseline (ZRB) is task-specific and the same as before.

Task	Normalization	ZRB	SVM	MLP	CNN
HC/GD	no norm.	68.0	-0.9	-1.0	-0.2
HC/GD	min-max	68.0	-1.1	-2.0	-0.5
HC/H	no norm.	62.6	-1.8	-2.1	-2.0
HC/H	min-max	62.6	-2.2	-3.7	-3.2
HC/K	no norm.	54.4	-1.8	-1.9	-0.7
HC/K	min-max	54.4	-4.1	-5.0	-2.1
HC/A	no norm.	59.0	-1.6	-1.8	-1.6
HC/A	min-max	59.0	1.2	0.9	-0.1

Do different classifiers rely on different patterns? A condensed comparison of the three employed classification methods is depicted in Figure 6. The LRP relevance values are consistent for both normalization modalities. For non-normalized data (*e.g.,* for task HC/GD see Supplementary Figures S 1, S 3, and S 5), the relevant regions for SVM and MLP largely correspond across all binary classification tasks. The CNN matches the relevant regions of SVM and MLP in broad terms. The relevant regions in F_V of the unaffected side for the CNN are considerably lower compared to SVM and MLP (compare Supplementary Figures S 1, S 3, and S 5), *e.g.,* for task HC/GD the valley of the unaffected side is hardly relevant and the second peak of the unaffected side is considerably less relevant compared to SVM and

MLP. For min-max normalized data (see Figure 6), the relevant regions for SVM and MLP coincide also to a large extent. The relevant regions of CNN correspond to those of SVM and MLP with regard to their location, but are considerably more relevant (best visible in the total relevance curves in the right part of Figure 6). The most pronounced difference between the classification methods can be observed in the input relevance curves at the beginning and the end of F_V. While LRP indicates that those regions are relevant for SVM and MLP, the total relevance curve of the CNN does not show any correspondence in those regions.

The remaining binary classification tasks, *i.e.,* HC/H (see Supplementary Figures S 7–S 12), HC/K (see Supplementary Figures S 13–S 18) and HC/A (see Supplementary Figures S 19–S 24) generally confirm the discussed findings.

Overall, with regard to our second research direction, XAI shows clearly the importance of data normalization for obtaining unbiased explanations. Furthermore, XAI allows to compare classifiers and the patterns they rely on, even though some patterns are difficult to interpret (*e.g.,* the strongly relevant patterns at the beginning and the end of F_V for SVM and MLP). The beginning and the end of the stance phase are characterized by a higher degree of inter- and intra-subject variability (Bizovska et al., 2014). In the absence of ground truth information for automatically generated explanations, it is difficult to assess whether these relevant regions for SVM and MLP are related to meaningful gait characteristics (*i.e.,*, which are particularly evident in the more "unstable" initial and final stance phases with respect to balance) or bias (*i.e.,* related to the recording or processing of the GRF signals). Although XAI cannot explain these patterns in detail, it enables to identify and compare the learning strategies of different classification methods and thus to point out potential degenerations, influences of noise and spurious correlations.

5.3 Statistical Evaluation of Decision Explanations using Statistical Parameter Mapping

In the following, we compare the regions found to be statistically significantly different by SPM and those with high relevance estimates using LRP. Our expectation was that these regions are related to some degree, as statistically significantly different features are more likely to be beneficial for classification. In the vast majority of cases, the SPM analysis shows statistically significant differences in regions which are also highly relevant for classification. Thus, for binary classification tasks, machine learning models base their predictions primarily on features that are significantly different between these two classes. This can be observed in the HC/GD classification for both, min-max normalized and non-normalized GRF signals, *i.e.,* as the total relevance increases, the effect size usually also increases (see Figure 4D and Figure 5D).

However, it is again noticeable that especially for the classification of non-normalized GRF signals, considerably fewer features are relevant for machine learning models than the SPM analysis identified as statistically different. In this context, the SPM analysis proofs to be a reliable reference for XAI approaches, since it is invariant to input data normalization and value ranges. For non-normalized signals the SPM provided a valuable indication for the presence of a bias. While LRP was not able to declare certain regions in the shear forces as relevant (actually due to biased machine learning models, not an insufficiency of LRP), SPM clearly showed that there are statistically validated differences.

As mentioned above, input normalization leads to an increased number of relevant regions. Furthermore, there is a greater overlap between the results of LRP and SPM for the classification of min-max normalized data. This also implies an advantage in the use of normalized input vectors for gait classification (even though for the present dataset the classification accuracy does not increase), which is in accordance with machine learning literature (Hsu et al., 2016; Chollet, 2017).

5.4 Clinical Evaluation of Decision Explanations

The visualizations of the derived classification results from min-max normalized data illustrate certain clinically meaningful patterns. For classification task HC/A (see Supplementary Figure S 20) one can identify pronounced peaks in the total relevance curves of F_{AP} of the affected and unaffected side. These regions are highly relevant for the classification purpose as indicated by LRP. From a clinical perspective this observation seems plausible as an impaired ankle joint is likely to impact forward step propulsion in the terminal stance (TS) phase due to a limited range of motion, reduced muscle strength, and/or the presence of pain. As a consequence, also the contralateral (unaffected) side shows aberrations in F_{AP} regarding the initial contact (IC) of the foot caused by the lower impulse that was generated by the affected side.

In contrast, for classification task HC/K highest LRP relevance values are present in F_V and F_{AP} (see Supplementary Figure S 14). Changes in F_V may result from a lessened knee flexibility that hinders typical knee dynamics over the entire course of the stance phase. More precisely, healthy walking requires a fully extended knee joint during IC and a slight knee flexion thereafter causing a relief of body weight during the mid stance (MS) phase by definition called loading response. Moreover, further knee extension is essential to enable forward propulsion in late MS and TS, which may be insufficient in case of a decreased range of motion in the knee joint and/or a lack of muscle strength. These altered dynamics also affect GRF measurements in F_{AP} similar to those described above for the ankle joint, specifically observable during IC due to a possible flattened foot position and in TS caused by a reduced forward propulsion.

Highest LRP relevance values for the classification task HC/H are obtained during IC in F_V of the affected side and in F_{AP} of the unaffected side (see Supplementary Figure S 8). These results may be ascribed to lowered impact and weight bearing in the early stance phase (due to a more cautious walking strategy) in order to avoid excessive load on the affected hip joint. Furthermore, the lowered braking impulse in F_{AP} on the unaffected side can be traced back to a lowered forward propulsion induced by a possible insufficient hip extension on the affected side. However, in contrast to LRP results of the knee joint, relevance values for MS in F_V are low in this specific task. This particular observation could be explained by the role of the knee and ankle joint, which are essential to generate typical gait dynamics in MS, but should not be restricted to people with hip impairments.

The classification task HC/GD (see Figure 5) highlights once again the significance of the IC (F_V of affected side and F_{AP} of unaffected side), which is relevant for classification purposes across all groups. Other relevant areas – even if not as distinctive – reflect the general characteristics that were already presented within the pairwise comparisons described above, such as a pronounced second peak and altered gait dynamics in MS of F_V as well as a lessened forward propulsion in F_{AP} of the affected side.

As the results presented above are based on min-max normalized data, the question arises whether similar observations can be derived without normalization. The decision explanations for non-normalized data (see Figure 4 and Supplementary Figures S 7, S 13, S 19) clearly show a different picture, even if classification results are comparable to those obtained with min-max normalized data. Relevant regions can only be found in F_V of the GRFs. These observations again highlight the fact that normalization affects explainability and, therefore, needs to be considered also from a clinical viewpoint. However, with regard to our first research direction it can be concluded that the employed classifiers, which are trained on min-max normalized data, in combination with LRP serve well for identifying clinically relevant features.

6 CONCLUSION

The present findings highlight that complex machine learning models, such as CNNs, base their predictions on meaningful features of GRF signals in a clinical gait classification task (that are in accordance with a statistical and clinical evaluation). Hence, XAI methods which allow to explain the decisions of machine learning models, such as LRP, can be promising solutions to increase transparency of automatic classification predictions in CGA and can help to make the decision processes comprehensible to clinical and legal experts. Thereby, XAI may facilitate the application of AI-based decision-support systems in clinical practice. Within the scope of our analysis we were able to show that:

- Although the three classification methods investigated – CNN, MLP and SVM – achieved similar classification accuracies, minor differences can be observed in the regions that are relevant for their predictions. In addition, CNNs showed the greatest agreement with the statistical and clinical evaluation.

- Input data normalization allows machine learning models to consider features from various input signals for their predictions (especially if the value ranges differ as much as for the three force components of the GRF). Without normalization, only relevant regions in the F_V were identified.

- Highly relevant regions were identified in the signals of the affected and unaffected side. Thus, the unaffected side captures additional information which are relevant for automated gait classifications.

- For the investigated binary gait classification tasks, machine learning models seem to learn an over-complete set of features that may contain redundant information. This might explain why the occlusion of shear forces had negligible influence on the classification accuracies and also why the classification accuracies for the classification of normalized and non-normalized GRF signals were comparable.

However, the present paper can only be considered as a first step towards this direction. Further research is necessary in order to compare different decision explanation methods and rules (Kohlbrenner et al., 2019) for different classification tasks and datasets. In addition, quantitative methods are needed to assess the quality of decision explanations (Samek et al., 2017). For time-series data such as GRFs, SPM proved to be a suitable statistical reference for XAI methods.

CONFLICT OF INTEREST STATEMENT

FUNDING

ACKNOWLEDGMENTS

DATA AVAILABILITY STATEMENT

For our analysis, we used a subset of a large dataset that is currently being prepared for an open-source publication as the GAITREC dataset in an online repository. The data and the experimental code will be made publicly available on GitHub after publication.

REFERENCES

Adadi, A. and Berrada, M. (2018). Peeking inside the black-box: A survey on explainable artificial intelligence (XAI). *IEEE Access* 6, 52138–52160. doi:10.1109/ACCESS.2018.2870052

Alaqtash, M., Sarkodie-Gyan, T., Yu, H., Fuentes, O., Brower, R., and Abdelgawad, A. (2011). Automatic classification of pathological gait patterns using ground reaction forces and machine learning algorithms. In *2011 Annual International Conference of the IEEE Engineering in Medicine and Biology Society (EMBS)* (IEEE), 453–457. doi:10.1109/IEMBS.2011.6090063

Arya, V., Bellamy, R. K., Chen, P.-Y., Dhurandhar, A., Hind, M., Hoffman, S. C., et al. (2019). One explanation does not fit all: A toolkit and taxonomy of ai explainability techniques. *arXiv:1909.03012 [Preprint].* Available at: https://arxiv.org/abs/1909.03012

Bach, S., Binder, A., Montavon, G., Klauschen, F., Müller, K.-R., and Samek, W. (2015). On pixel-wise explanations for non-linear classifier decisions by layer-wise relevance propagation. *PloS one* 10, e0130140. doi:10.1371/journal.pone.0130140

Baehrens, D., Schroeter, T., Harmeling, S., Kawanabe, M., Hansen, K., and Müller, K.-R. (2010). How to explain individual classification decisions. *Journal of Machine Learning Research* 11, 1803–1831.

Balduzzi, D., Frean, M., Leary, L., Lewis, J. P., Ma, K. W.-D., and McWilliams, B. (2017). The shattered gradients problem: If resnets are the answer, then what is the question? In *Proceedings of the 34th International Conference on Machine Learning* (PMLR), 342–350.

Bizovska, L., Svoboda, Z., Kutilek, P., Janura, M., Gaba, A., and Kovacikova, Z. (2014). Variability of centre of pressure movement during gait in young and middle-aged women. *Gait & Posture* 40, 399 – 402. doi:https://doi.org/10.1016/j.gaitpost.2014.05.065

Chau, T. (2001). A review of analytical techniques for gait data. Part 1: fuzzy, statistical and fractal methods. *Gait & Posture* 13, 49–66. doi:10.1016/S0966-6362(00)00094-1

Chollet, F. (2017). *Deep learning with Python*. Shelter Island (NY): Manning Publications Company

Cireşan, D., Meier, U., Masci, J., and Schmidhuber, J. (2012). Multi-column deep neural network for traffic sign classification. *Neural Networks* 32, 333–338. doi:10.1016/j.neunet.2012.02.023

Esteva, A., Kuprel, B., Novoa, R. A., Ko, J., Swetter, S. M., Blau, H. M., et al. (2017). Dermatologist-level classification of skin cancer with deep neural networks. *Nature* 542, 115–118. doi:10.1038/nature21056

European Union (2016). Regulation (EU) 2016/679 of the european parliament and of the council of 27 april 2016 on the protection of natural persons with regard to the processing of personal data and on the free movement of such data, and repealing directive 95/46/ec (General Data Protection Regulation). *Official Journal of the European Union* L 119, 1–88. Available at: https://eur-lex.europa.eu/eli/reg/2016/679/oj

Figueiredo, J., Santos, C. P., and Moreno, J. C. (2018). Automatic recognition of gait patterns in human motor disorders using machine learning: A review. *Medical Engineering and Physics* 53, 1–12. doi:10.1016/j.medengphy.2017.12.006

Fong, R. C. and Vedaldi, A. (2017). Interpretable explanations of black boxes by meaningful perturbation. In *2017 IEEE International Conference on Computer Vision (ICCV)* (IEEE), 3429–3437. doi:10.1109/ICCV.2017.371

Halilaj, E., Rajagopal, A., Fiterau, M., Hicks, J. L., Hastie, T. J., and Delp, S. L. (2018). Machine learning in human movement biomechanics: Best practices, common pitfalls, and new opportunities. *Journal of Biomechanics* 81, 1–11. doi:10.1016/j.jbiomech.2018.09.009

He, J., Baxter, S. L., Xu, J., Xu, J., Zhou, X., and Zhang, K. (2019). The practical implementation of artificial intelligence technologies in medicine. *Nature Medicine* 25, 30–36. doi:10.1038/s41591-018-0307-0

Hendricks, L. A., Akata, Z., Rohrbach, M., Donahue, J., Schiele, B., and Darrell, T. (2016). Generating visual explanations. In *European Conference on Computer Vision (ECCV)* (Springer), 3–19. doi:10.1007/978-3-319-46493-0_1

Holzinger, A., Biemann, C., Pattichis, C. S., and Kell, D. B. (2017). What do we need to build explainable AI systems for the medical domain? *arXiv:1712.09923 [Preprint]*. Available at: https://arxiv.org/abs/1712.09923

Holzinger, A., Langs, G., Denk, H., Zatloukal, K., and Müller, H. (2019). Causability and explainability of artificial intelligence in medicine. *Wiley Interdisciplinary Reviews: Data Mining and Knowledge Discovery* 9, e1312. doi:10.1002/widm.1312

Horst, F., Lapuschkin, S., Samek, W., Müller, K.-R., and Schöllhorn, W. I. (2019). Explaining the unique nature of individual gait patterns with deep learning. *Scientific Reports* 9, 2391. doi:10.1038/s41598-019-38748-8

Hsu, C. W., Chang, C. C., and Lin, C.-J. (2016). *A practical guide to support vector classification*. Technical report, National Taiwan University. Available at: https://www.csie.ntu.edu.tw/ cjlin/papers/guide/guide.pdf

Kohlbrenner, M., Bauer, A., Nakajima, S., Binder, A., Samek, W., and Lapuschkin, S. (2019). Towards best practice in explaining neural network decisions with lrp. *arXiv:1910.09840 [Preprint]*. Available at: http://arxiv.org/abs/1910.09840

Lapuschkin, S., Wäldchen, S., Binder, A., Montavon, G., Samek, W., and Müller, K.-R. (2019). Unmasking clever hans predictors and assessing what machines really learn. *Nature Communications* 10, 1096. doi:10.1038/s41467-019-08987-4

Lau, H.-y., Tong, K.-y., and Zhu, H. (2009). Support vector machine for classification of walking conditions of persons after stroke with dropped foot. *Human Movement Science* 28, 504–514. doi:10.1016/j.humov.2008.12.003

LeCun, Y., Bottou, L., Orr, G. B., and Müller, K.-R. (2012). Efficient backprop. In *Neural Networks: Tricks of the Trade - Second Edition* (Springer). 9–48. doi:10.1007/978-3-642-35289-8_3

Lundberg, S. M. and Lee, S.-I. (2017). A unified approach to interpreting model predictions. In *Advances in Neural Information Processing Systems (NIPS)* (Curran Associates, Inc.), 4765–4774. Available at: http://papers.nips.cc/paper/7062-a-unified-approach-to-interpreting-model-predictions.pdf

Maaten, L. v. d. and Hinton, G. (2008). Visualizing data using t-sne. *Journal of Machine Learning Research* 9, 2579–2605.

Montavon, G., Binder, A., Lapuschkin, S., Samek, W., and Müller, K.-R. (2019). Layer-wise relevance propagation: An overview. In *Explainable AI: Interpreting, Explaining and Visualizing Deep Learning* (Springer), 193–209. doi:10.1007/978-3-030-28954-6_10

Montavon, G., Samek, W., and Müller, K.-R. (2018). Methods for interpreting and understanding deep neural networks. *Digital Signal Processing* 73, 1–15. doi:10.1016/j.dsp.2017.10.011

Nguyen, A., Dosovitskiy, A., Yosinski, J., Brox, T., and Clune, J. (2016). Synthesizing the preferred inputs for neurons in neural networks via deep generator networks. In *Advances in Neural Information*

Processing Systems (Curran Associates, Inc.), 3387–3395. Available at: http://papers.nips.cc/paper/6519-synthesizing-the-preferred-inputs-for-neurons-in-neural-networks-via-deep-generator-networks.pdf

Nüesch, C., Valderrabano, V., Huber, C., von Tscharner, V., and Pagenstert, G. (2012). Gait patterns of asymmetric ankle osteoarthritis patients. *Clinical Biomechanics* 27, 613–618. doi:10.1016/j.clinbiomech.2011.12.016

Pataky, T. C. (2010). Generalized n-dimensional biomechanical field analysis using statistical parametric mapping. *Journal of Biomechanics* 43, 1976–1982. doi:10.1016/j.jbiomech.2010.03.008

Pataky, T. C. (2012). One-dimensional statistical parametric mapping in python. *Computer Methods in Biomechanics and Biomedical Engineering* 15, 295–301. doi:10.1080/10255842.2010.527837

Phinyomark, A., Petri, G., Ibáñez-Marcelo, E., Osis, S. T., and Ferber, R. (2018). Analysis of big data in gait biomechanics: Current trends and future directions. *Journal of Medical and Biological Engineering* 38, 244–260. doi:10.1007/s40846-017-0297-2

Ribeiro, M. T., Singh, S., and Guestrin, C. (2016). Model-agnostic interpretability of machine learning. *arXiv:1606.05386 [Preprint]*. Available at: http://arxiv.org/abs/1606.05386

Rosenthal, R. (1986). Meta-Analytic Procedures for Social Science Research Sage Publications: Beverly Hills, 1984, 148 pp. *Educational Researcher* 15, 18–20. doi:10.3102/0013189X015008018

Samek, W., Binder, A., Montavon, G., Lapuschkin, S., and Müller, K.-R. (2017). Evaluating the visualization of what a deep neural network has learned. *IEEE Transactions on Neural Networks and Learning Systems* 28, 2660–2673. doi:10.1109/TNNLS.2016.2599820

Samek, W., Wiegand, T., and Müller, K.-R. (2017). Explainable artificial intelligence: Understanding, visualizing and interpreting deep learning models. *ITU Journal: ICT Discoveries* 1, 39–48

Schöllhorn, W. I. (2004). Applications of artificial neural nets in clinical biomechanics. *Clinical Biomechanics* 19, 876–898. doi:10.1016/j.clinbiomech.2004.04.005

Shrikumar, A., Greenside, P., and Kundaje, A. (2017). Learning important features through propagating activation differences. In *Proceedings of the 34th International Conference on Machine Learning* (PMLR), 3145–3153.

Simonyan, K., Vedaldi, A., and Zisserman, A. (2013). Deep inside convolutional networks: Visualising image classification models and saliency maps. *arXiv:1312.6034 [Preprint]*. Available at: http://arxiv.org/abs/1312.6034

Slijepcevic, D., Zeppelzauer, M., Gorgas, A.-M., Schwab, C., Schüller, M., Baca, A., et al. (2017). Automatic classification of functional gait disorders. *IEEE Journal of Biomedical and Health Informatics* 22, 1653–1661. doi:10.1109/JBHI.2017.2785682

Slijepcevic, D., Zeppelzauer, M., Schwab, C., Raberger, A., Dumphart, B., Baca, A., et al. (2018). P 011-Towards an optimal combination of input signals and derived representations for gait classification based on ground reaction force measurements. *Gait & Posture* 65, 249. doi:10.1016/j.gaitpost.2018.06.155

Slijepcevic, D., Zeppelzauer, M., Schwab, C., Raberger, A.-M., Breiteneder, C., and Horsak, B. (2019). Input Representations and Classification Strategies for Automated Human Gait Analysis. *Gait & Posture* doi:https://doi.org/10.1016/j.gaitpost.2019.10.021

Štrumbelj, E. and Kononenko, I. (2014). Explaining prediction models and individual predictions with feature contributions. *Knowledge and Information Systems* 41, 647–665. doi:10.1007/s10115-013-0679-x

Tjoa, E. and Guan, C. (2019). A survey on explainable artificial intelligence (xai): Towards medical xai. *arXiv:1907.07374 [Preprint]*. Available at: https://arxiv.org/abs/1907.07374

Tonekaboni, S., Joshi, S., McCradden, M. D., and Goldenberg, A. (2019). What clinicians want: Contextualizing explainable machine learning for clinical end use. *arXiv:1905.05134 [Preprint].* Available at: https://arxiv.org/abs/1905.05134

Topol, E. J. (2019). High-performance medicine: The convergence of human and artificial intelligence. *Nature Medicine* 25, 44–56. doi:10.1038/s41591-018-0300-7

Turner, R. (2016). A model explanation system: Latest updates and extensions. *arXiv:1606.09517 [Preprint].* Available at: http://arxiv.org/abs/1606.09517

Van Gestel, L., De Laet, T., Di Lello, E., Bruyninckx, H., Molenaers, G., Van Campenhout, A., et al. (2011). Probabilistic gait classification in children with cerebral palsy: A Bayesian approach. *Research in Developmental Disabilities* 32, 2542–2552. doi:10.1016/j.ridd.2011.07.004

Wagner, M., Slijepcevic, D., Horsak, B., Rind, A., Zeppelzauer, M., and Aigner, W. (2019). Kavagait: Knowledge-assisted visual analytics for clinical gait analysis. *IEEE Transactions on Visualization and Computer Graphics* 25, 1528–1542. doi:10.1109/TVCG.2017.2785271

Wahid, F., Begg, R. K., Hass, C. J., Halgamuge, S., and Ackland, D. C. (2015). Classification of Parkinson's Disease Gait Using Spatial-Temporal Gait Features. *IEEE Journal of Biomedical and Health Informatics* 19, 1794–1802. doi:10.1109/JBHI.2015.2450232

Wilhelm, N., Vögele, A., Zsoldos, R., Licka, T., Krüger, B., and Bernard, J. (2015). Furyexplorer: Visual-interactive exploration of horse motion capture data. In *Visualization and Data Analysis 2015* (International Society for Optics and Photonics), 93970F. doi:10.1117/12.2080001

Wolf, S., Loose, T., Schablowski, M., Döderlein, L., Rupp, R., Gerner, H. J., et al. (2006). Automated feature assessment in instrumented gait analysis. *Gait & Posture* 23, 331–338. doi:10.1016/j.gaitpost.2005.04.004

Zintgraf, L. M., Cohen, T. S., Adel, T., and Welling, M. (2017). Visualizing deep neural network decisions: Prediction difference analysis. *arXiv:1702.04595 [Preprint].* Available at: http://arxiv.org/abs/1702.04595

Zurada, J. M., Malinowski, A., and Cloete, I. (1994). Sensitivity analysis for minimization of input data dimension for feedforward neural network. In *Proceedings of IEEE International Symposium on Circuits and Systems (ISCAS)* (IEEE), 447–450. doi:10.1109/ISCAS.1994.409622

SUPPLEMENTARY MATERIAL
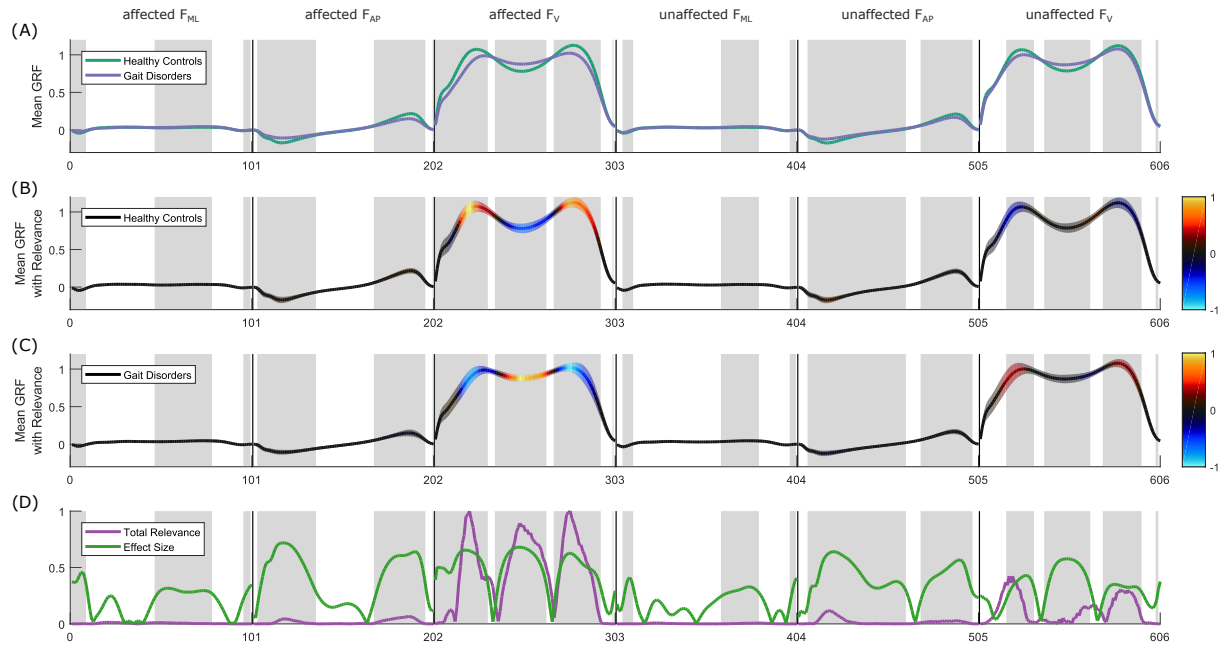
The present Supplementary Material is intended to present additional results we generated for the paper **"On the Understanding and Interpretation of Machine Learning Predictions in Clinical Gait Analysis Using Explainable Artificial Intelligence"**. The primary aim of this article is to investigate to which degree Explainable Artificial Intelligence (XAI) can increase the explainability and transparency of automatic decisions in the context of clinical gait analysis. In detail, this study exemplifies how XAI can be used to make clinical gait classification and prediction results understandable and traceable for clinical experts.

For this purpose, we define several gait classification tasks, employ a representative set of classifiers – (linear) Support Vector Machine (SVM), Multi-layer Perceptron (MLP), and Convolutional Neural Network (CNN) – and a well-established XAI method – Layer-wise Relevance Propagation (LRP) – to explain decision at the signal (input) level. In addition to an evaluation of the explanations by a clinical expert, as a second reference, we propose the use of Statistical Parameter Mapping (SPM) to verify the obtained results from a statistical point of view. The dataset employed, comprises ground reaction force (GRF) measurements from 132 patients with gait disorders (GD) and data from 62 healthy controls (HC). The GD class is furthermore differentiated into three classes of gait disorders associated with the hip (H), knee (K), and ankle (A). The classification tasks, which represent the basis of the XAI investigation, due to high classification accuracies obtained, include a binary classification between healthy controls and all gait disorders (HC/GD), and a binary classification between healthy controls and each gait disorder separately, *i.e.,*, HC/H, HC/K, and HC/A.
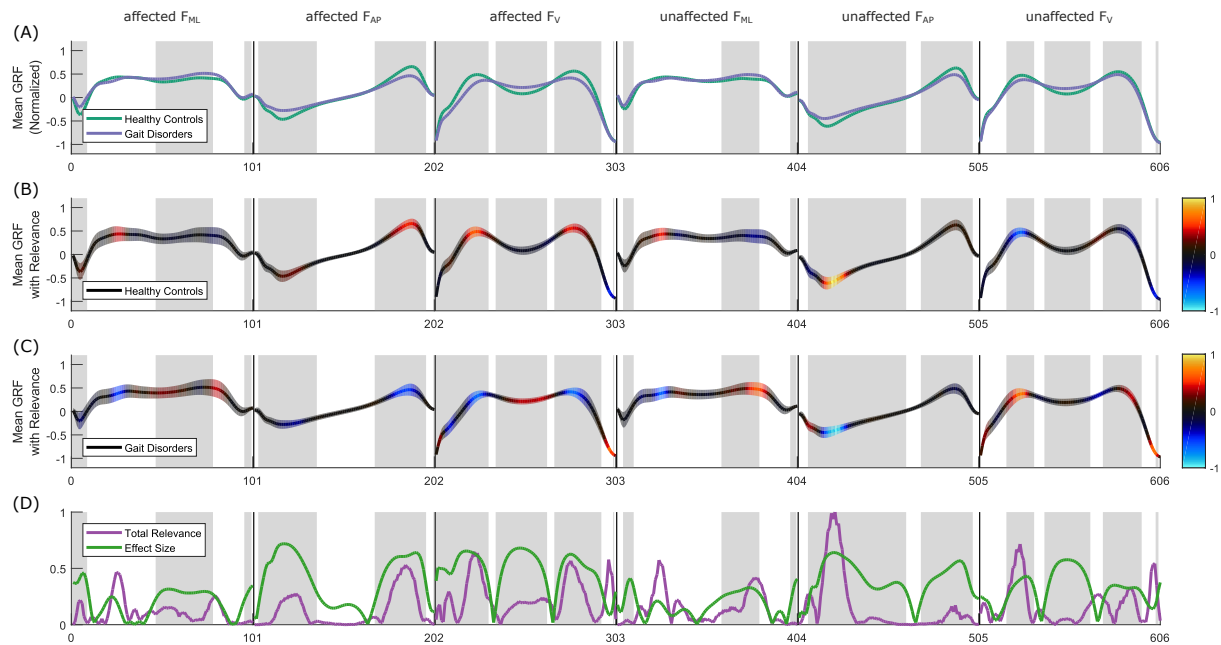
The following figures visualize decision explanation obtained with LRP. The input vector for the classifiers comprises concatenated affected and unaffected GRF signals. These GRF signals are time-normalized to 101 points (100% stance), thus the input vector contains 606 values. For each value LRP provides whether they are relevant or not for the classification. Sub-figure (A) shows mean GRF signals averaged over each class of the classification task. The shaded areas in all sub-figures highlight areas in the input signals where SPM resulted in a statistically significant difference between both classes. Sub-figure (B) shows mean GRF signals (including a band of one standard deviation) for the HC class. The input relevance indicates which GRF characteristics were most relevant for (or contradictory to) the classification of a certain class. For visualization, input values neutral to the prediction ($R_i \approx 0$) are shown in black, while warm hues indicate input values supporting the prediction ($R_i \gg 0$) of the analyzed class and cool hues identify contradictory input values ($R_i \ll 0$). Sub-figure (C) depicts mean GRF signals averaged over a pathological class (H, K, or A) or all gait disorders (GD), in the same format as in sub-figure (B). Sub-figure (D) shows the effect size obtained from SPM and the total relevance, which is calculated as the sum of the absolute input relevance values of both classes. The total relevance indicates the common relevance of the input signal for the classification task.

1 CLASSIFICATION TASK: HC/GD

1.1 Classifier: CNN
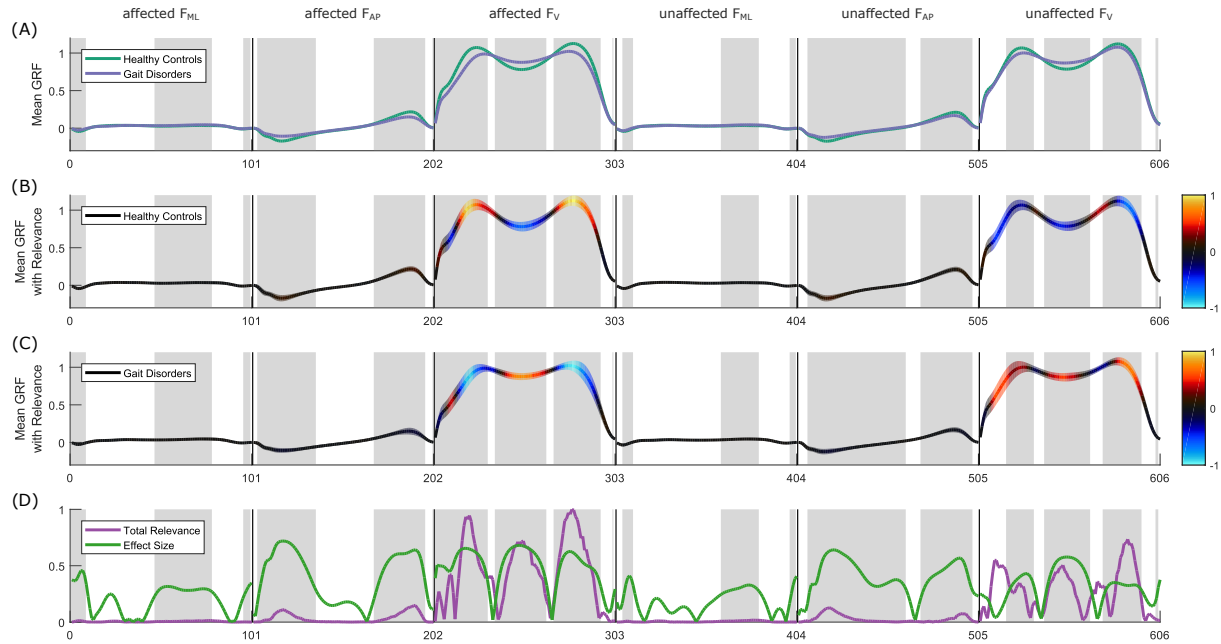
Supplementary Figure S 1. Result overview for the classification of healthy controls and the aggregated class of all three gait disorders (HC/GD) based on non-normalized GRF signals using a CNN as classifier.
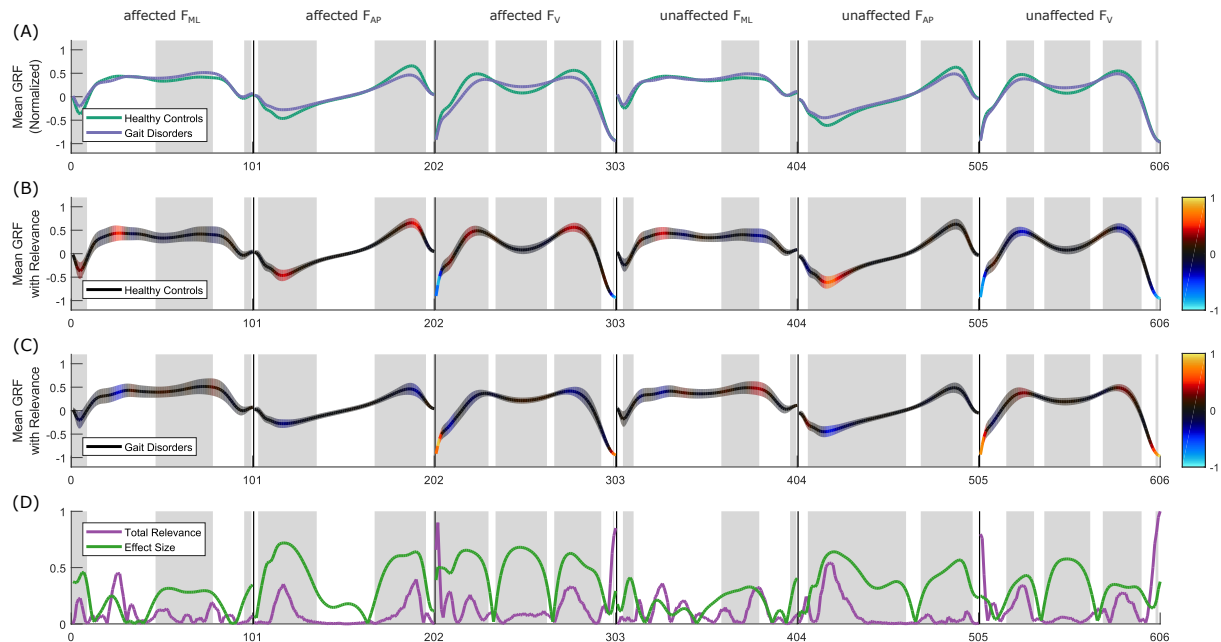

Supplementary Figure S 2. Result overview for the classification of healthy controls and the aggregated class of all three gait disorders (HC/GD) based on min-max normalized GRF signals using a CNN as classifier.

1.2 Classifier: MLP
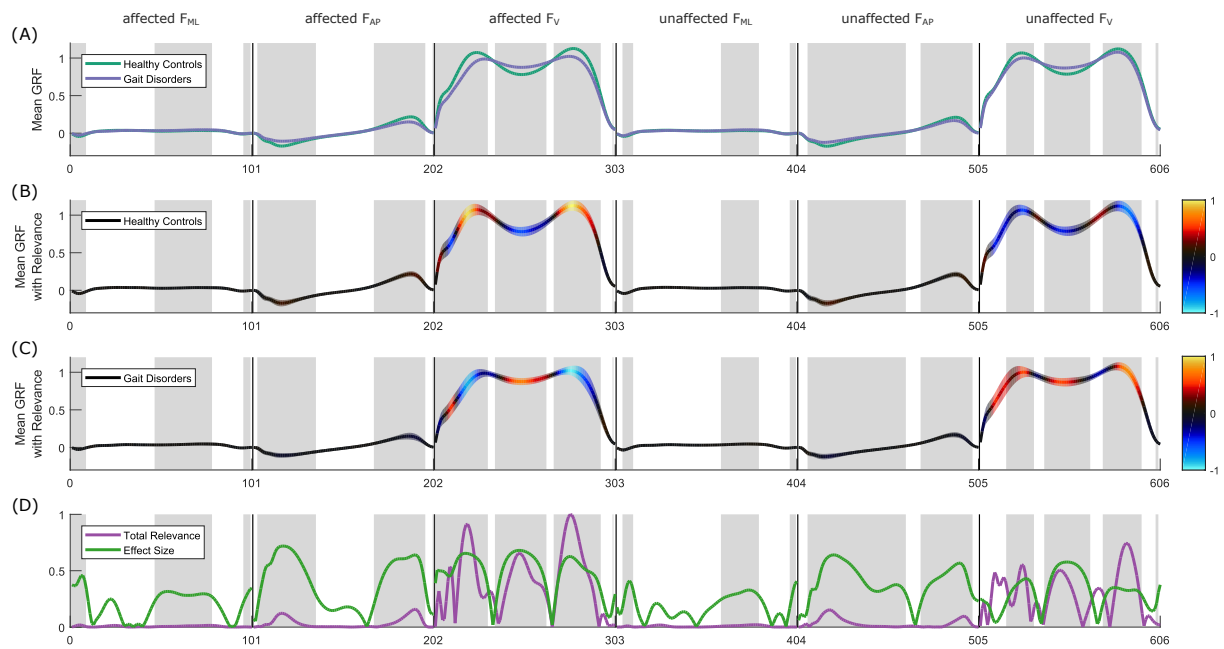
Supplementary Figure S 3. Result overview for the classification of healthy controls and the aggregated class of all three gait disorders (HC/GD) based on non-normalized GRF signals using a MLP as classifier.
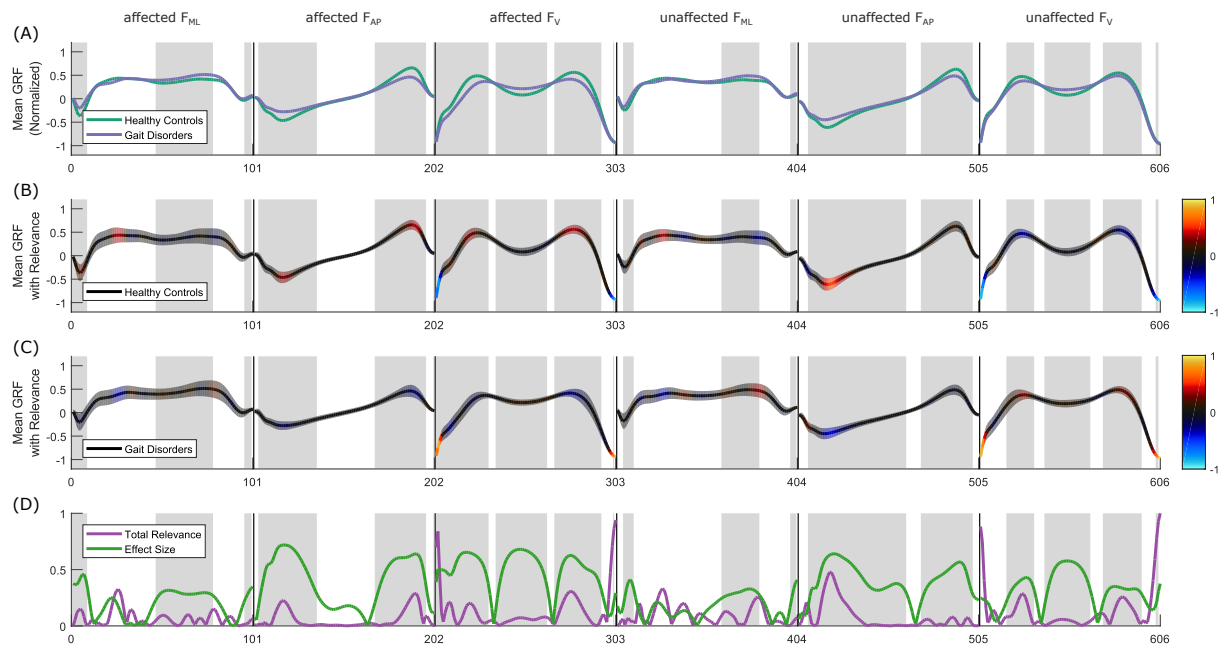
Supplementary Figure S 4. Result overview for the classification of healthy controls and the aggregated class of all three gait disorders (HC/GD) based on min-max normalized GRF signals using a MLP as classifier.

1.3 Classifier: SVM
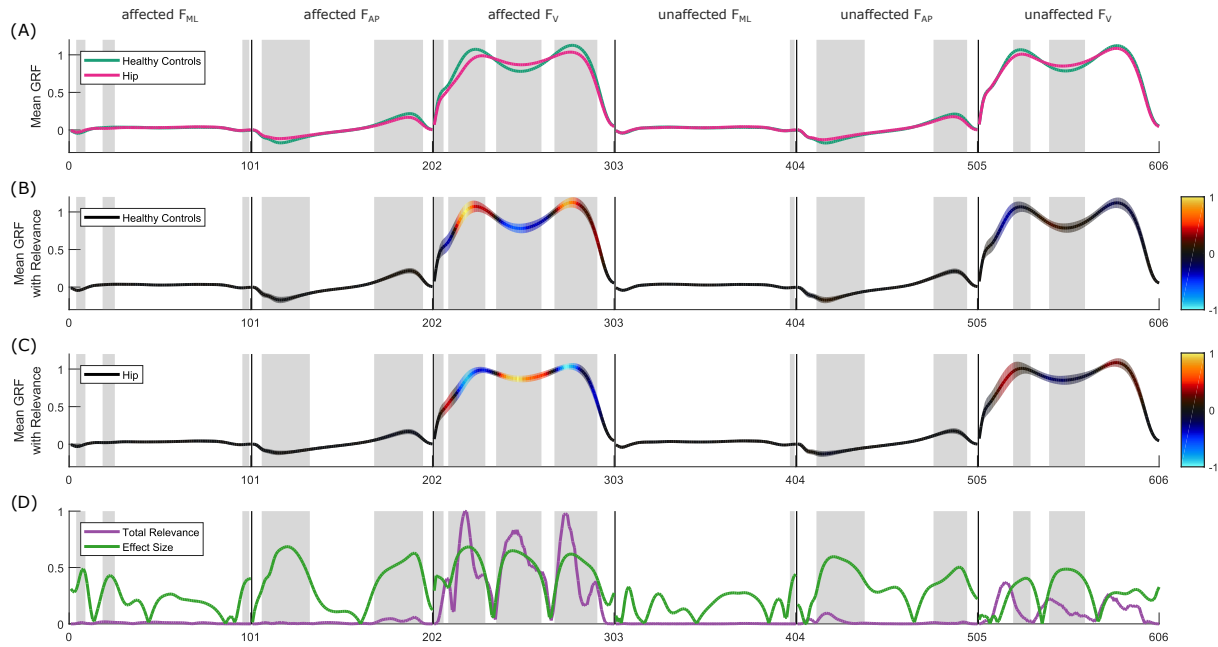
Supplementary Figure S 5. Result overview for the classification of healthy controls and the aggregated class of all three gait disorders (HC/GD) based on non-normalized GRF signals using a SVM as classifier.
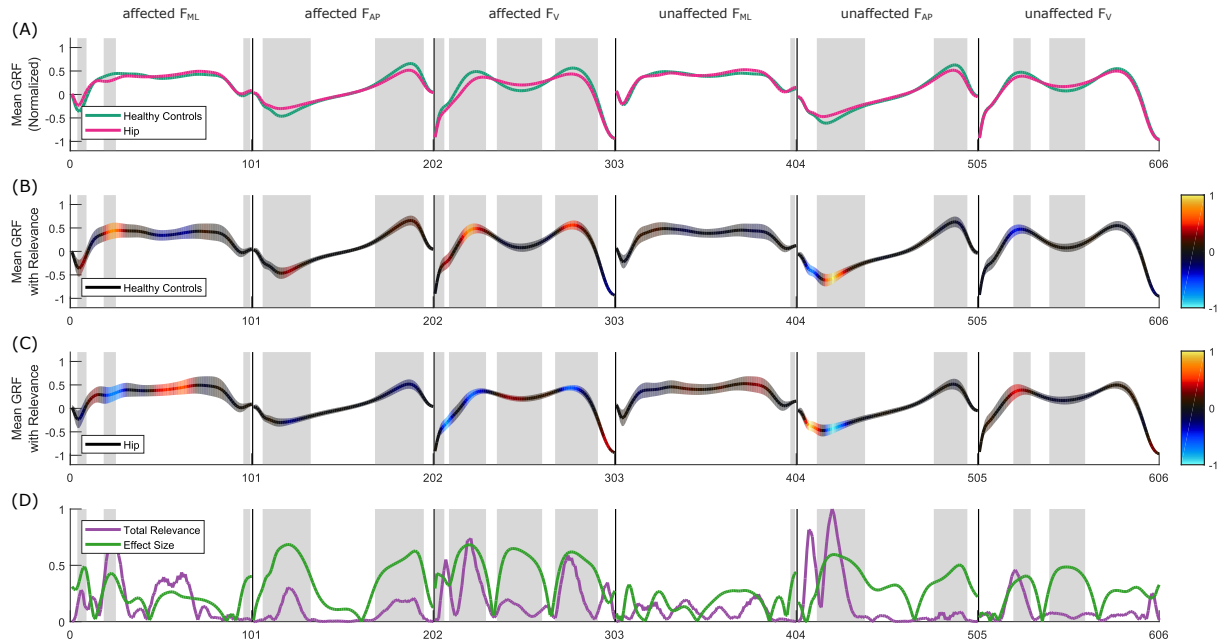
Supplementary Figure S 6. Result overview for the classification of healthy controls and the aggregated class of all three gait disorders (HC/GD) based on min-max normalized GRF signals using a SVM as classifier.

# 2 CLASSIFICATION TASK: HC/H

2.1 Classifier: CNN
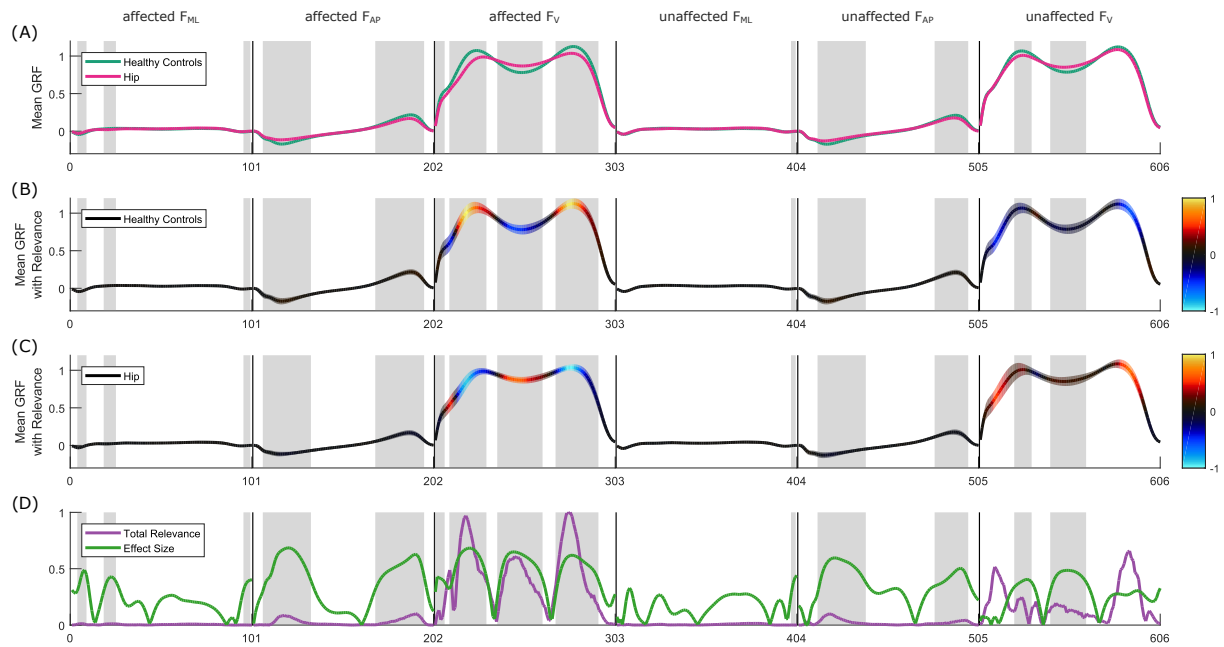
Supplementary Figure S 7. Result overview for the classification of healthy controls (HC) and hip injury class (H) based on non-normalized GRF signals using a CNN as classifier.
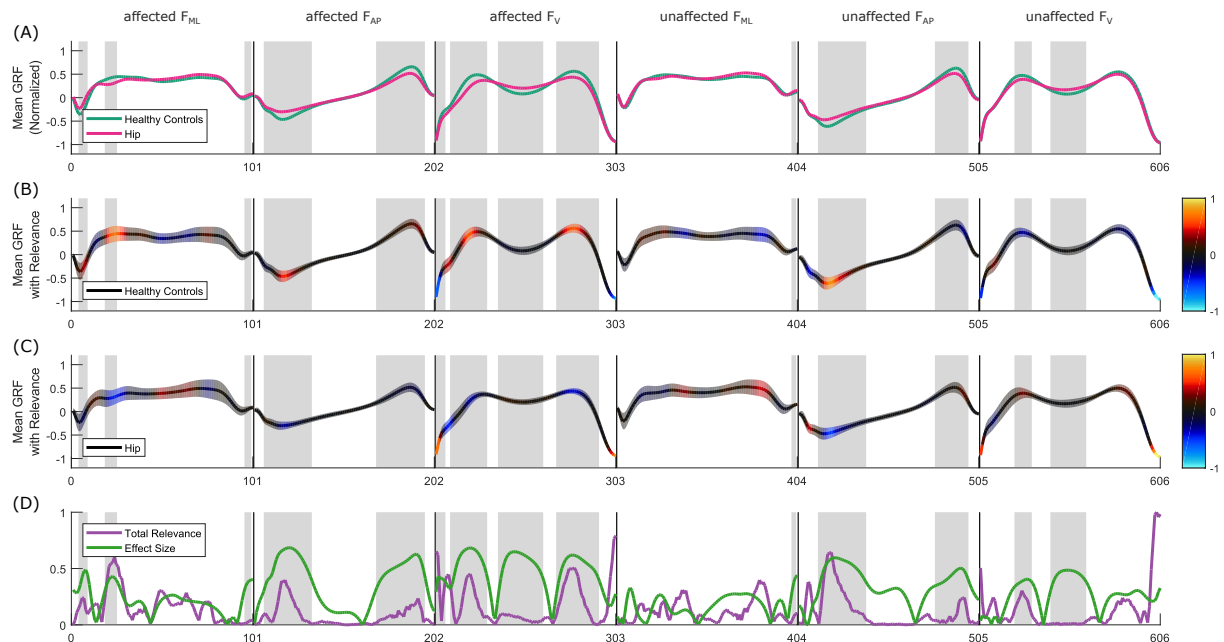

Supplementary Figure S 8. Result overview for the classification of healthy controls (HC) and hip injury class (H) based on min-max normalized GRF signals using a CNN as classifier.

2.2 Classifier: MLP
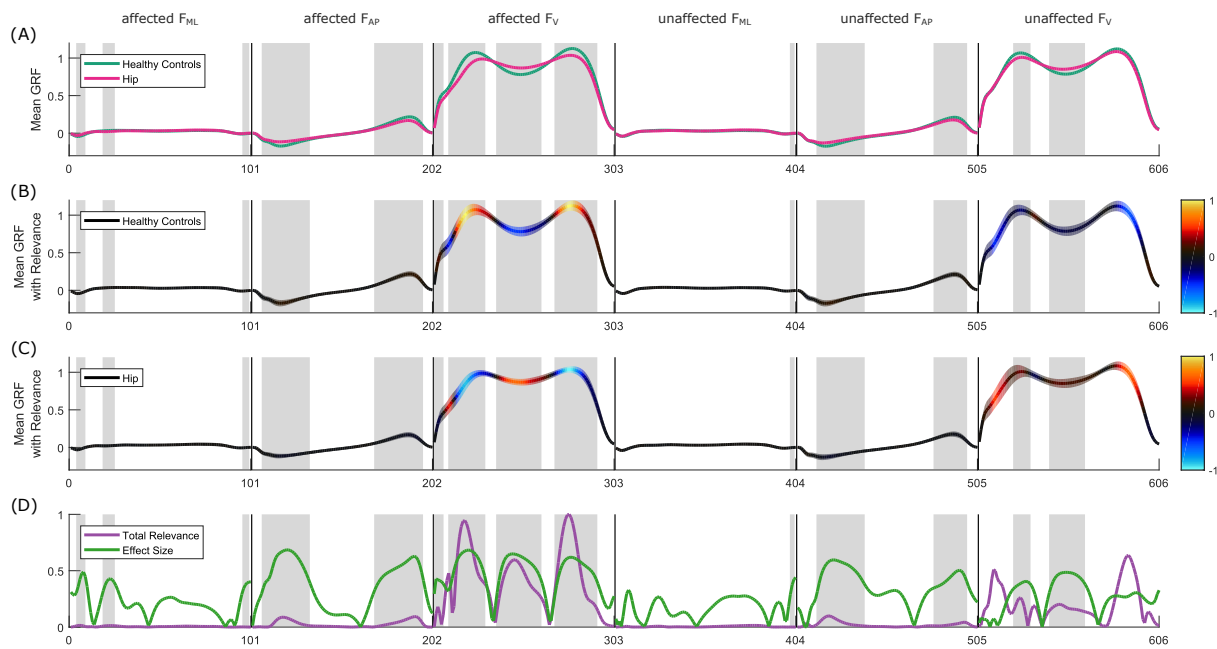
Supplementary Figure S 9. Result overview for the classification of healthy controls (HC) and hip injury class (H) based on non-normalized GRF signals using a MLP as classifier.
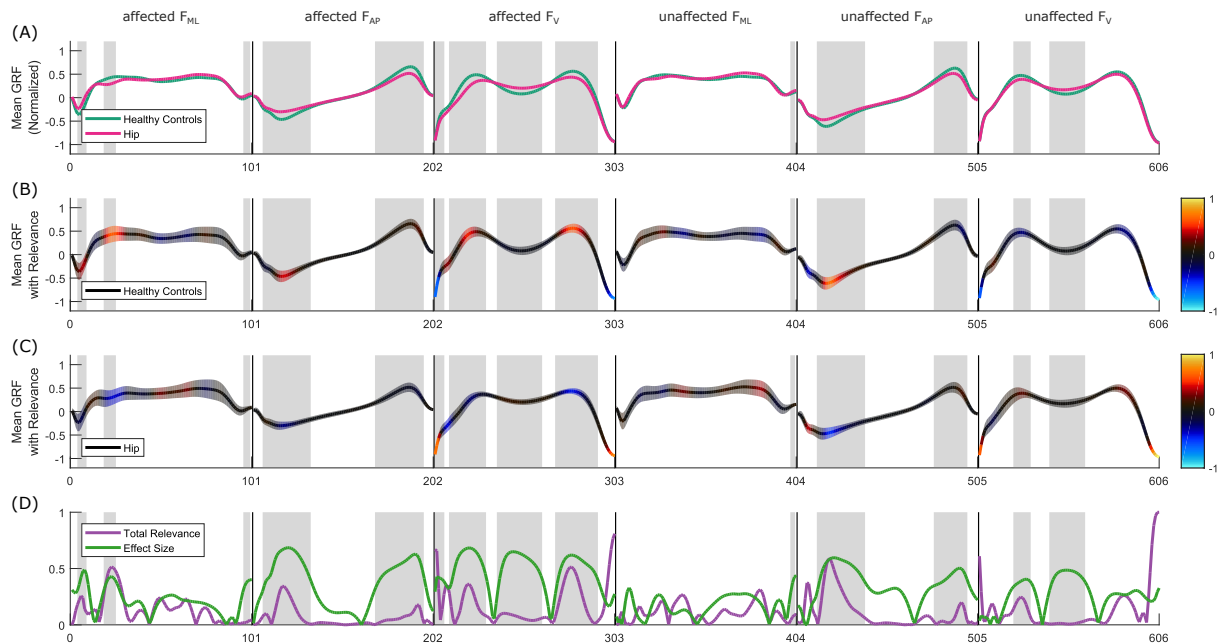
Supplementary Figure S 10. Result overview for the classification of healthy controls (HC) and hip injury class (H) based on min-max normalized GRF signals using a MLP as classifier.

2.3 Classifier: SVM
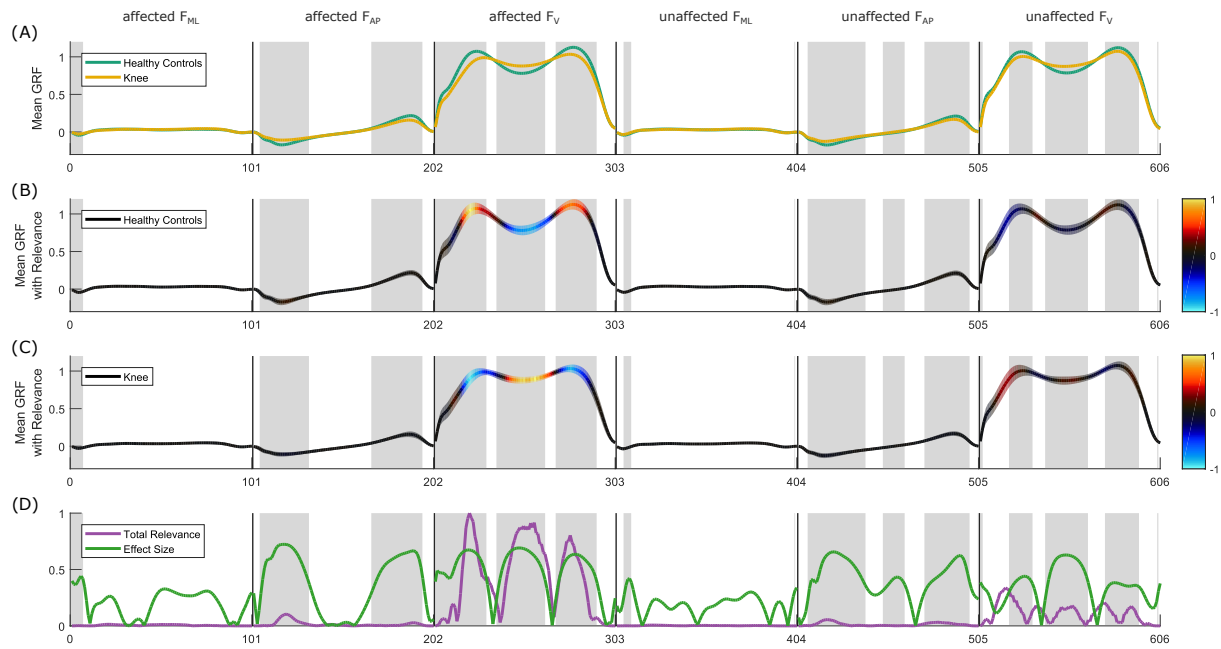
Supplementary Figure S 11. Result overview for the classification of healthy controls (HC) and hip injury class (H) based on non-normalized GRF signals using a SVM as classifier.
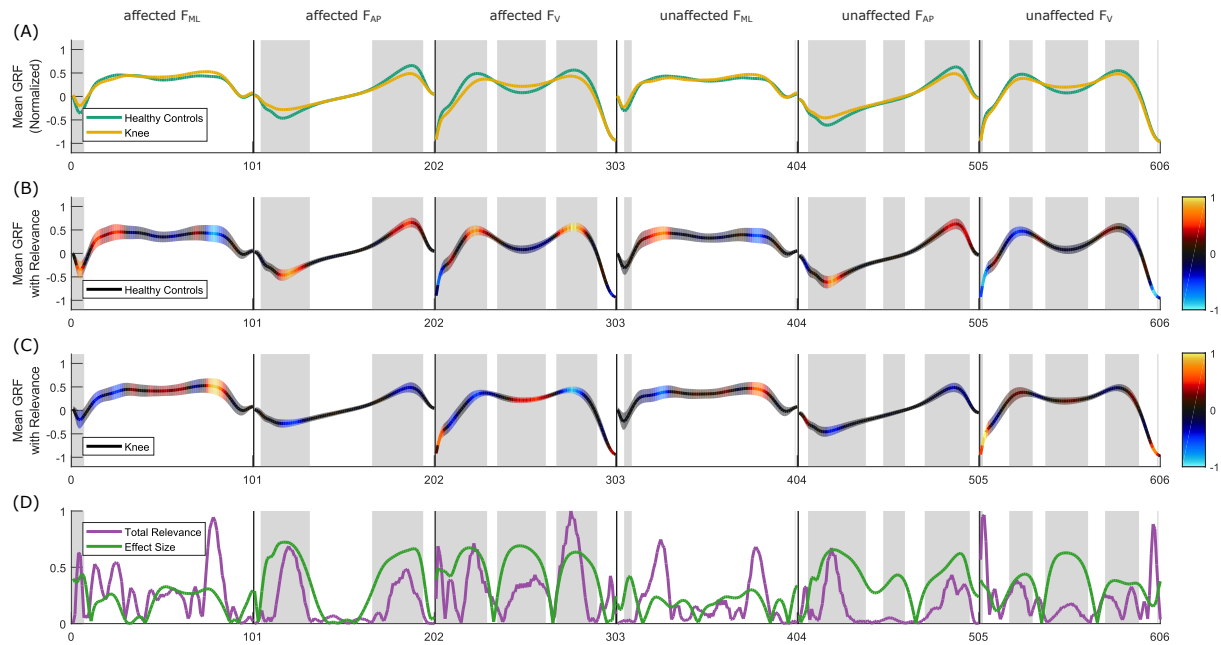

Supplementary Figure S 12. Result overview for the classification of healthy controls (HC) and hip injury class (H) based on min-max normalized GRF signals using a SVM as classifier.

3 CLASSIFICATION TASK: HC/K

3.1 Classifier: CNN
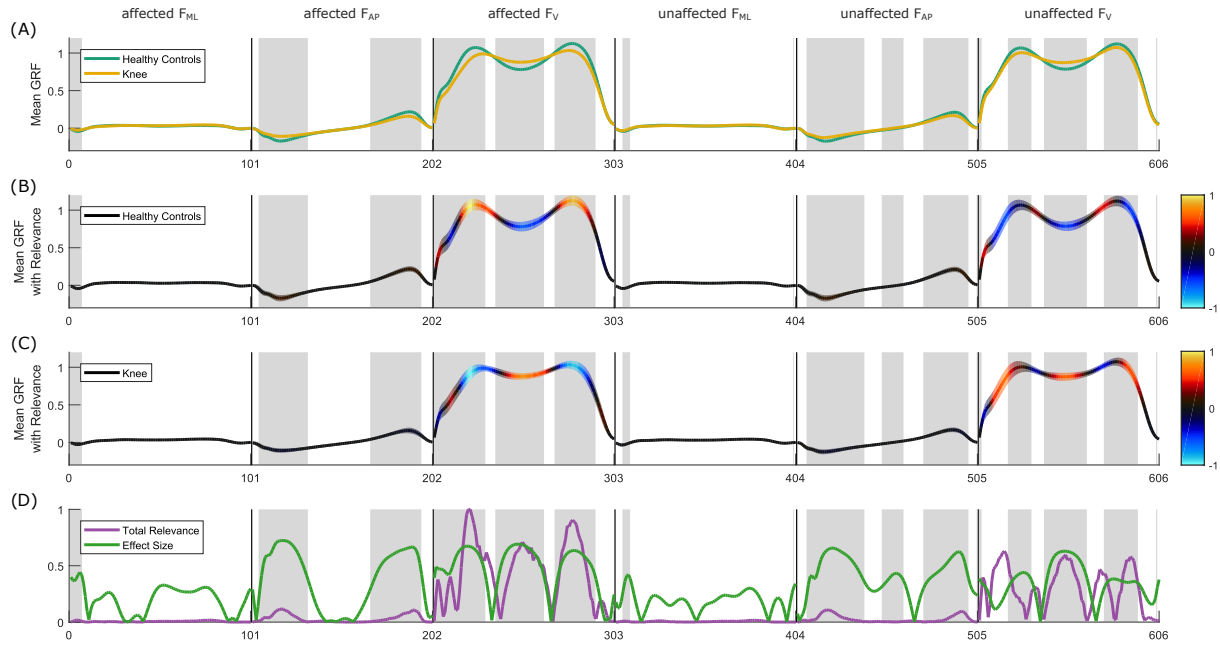
Supplementary Figure S 13. Result overview for the classification of healthy controls (HC) and knee injury class (K) based on non-normalized GRF signals using a CNN as classifier.
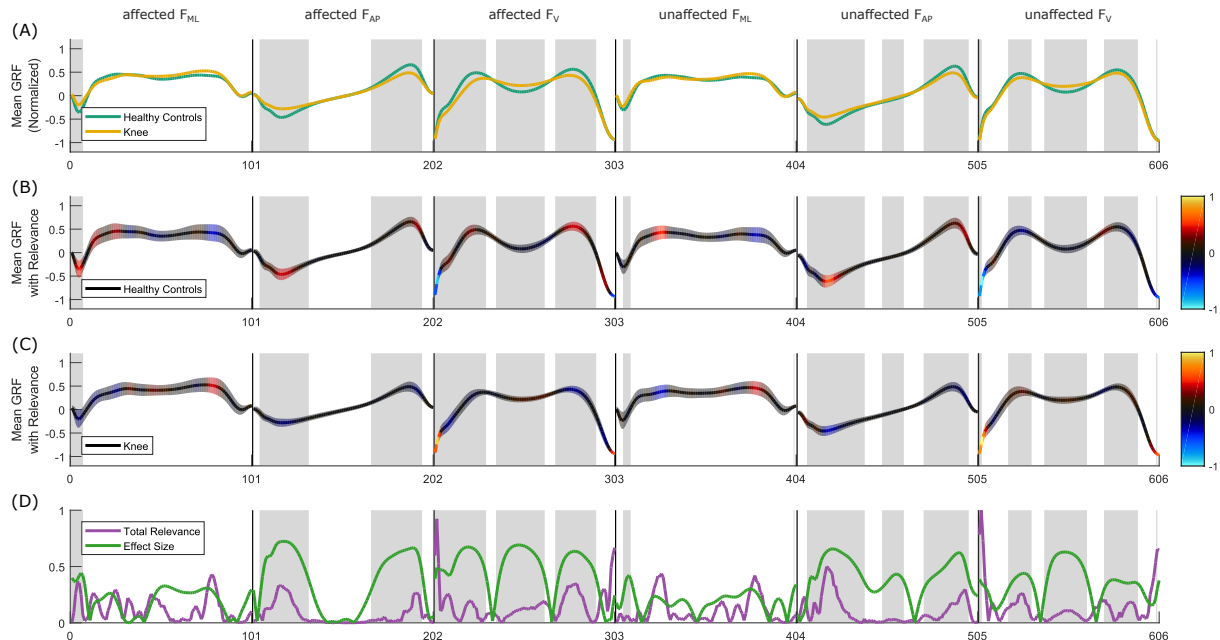
Supplementary Figure S 14. Result overview for the classification of healthy controls (HC) and knee injury class (K) based on min-max normalized GRF signals using a CNN as classifier.

3.2   Classifier: MLP
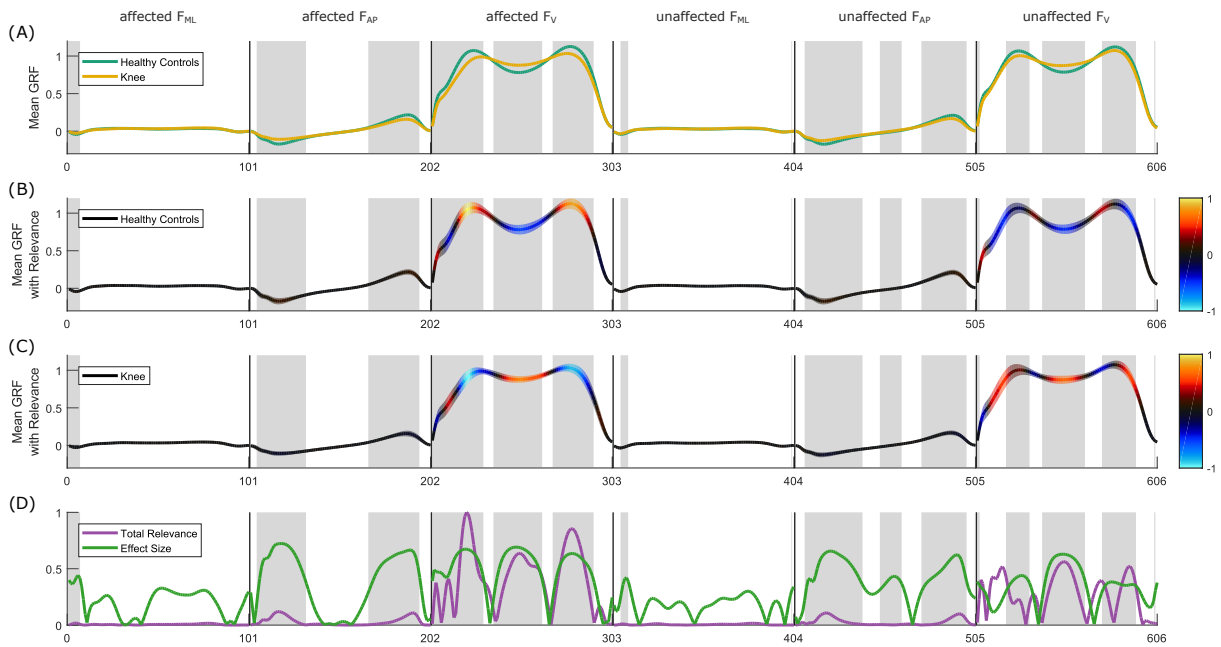
Supplementary Figure S 15. Result overview for the classification of healthy controls (HC) and knee injury class (K) based on non-normalized GRF signals using a MLP as classifier.
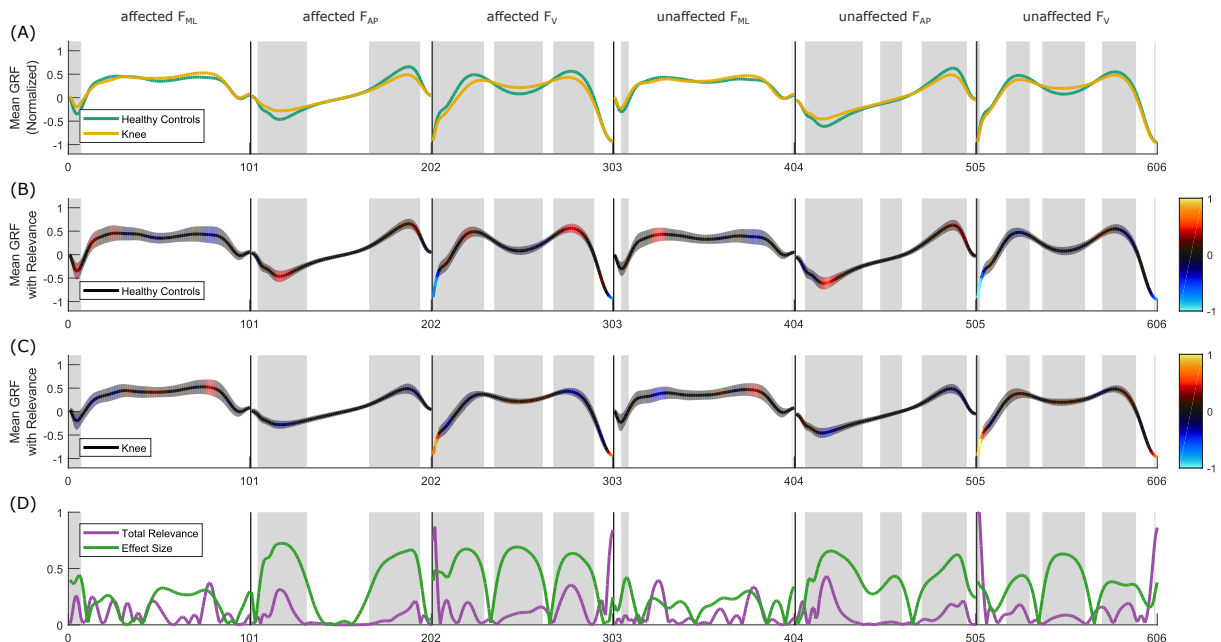

Supplementary Figure S 16. Result overview for the classification of healthy controls (HC) and knee injury class (K) based on min-max normalized GRF signals using a MLP as classifier.

3.3 Classifier: SVM
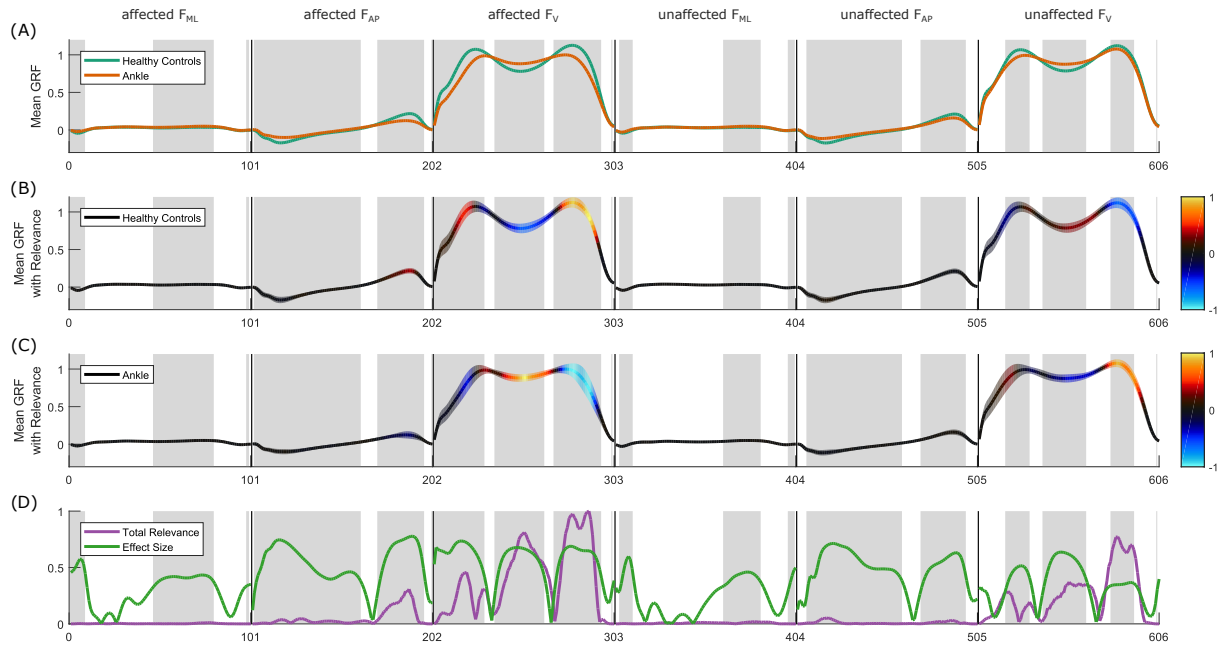
Supplementary Figure S 17. Result overview for the classification of healthy controls (HC) and knee injury class (K) based on non-normalized GRF signals using a SVM as classifier.
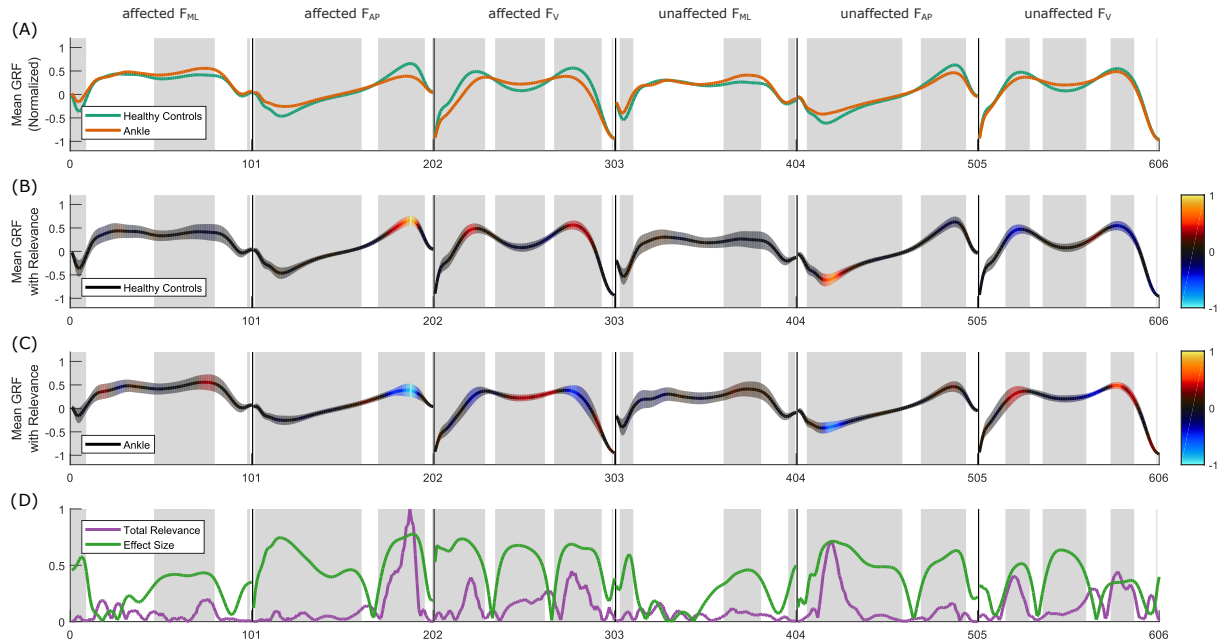
Supplementary Figure S 18. Result overview for the classification of healthy controls (HC) and knee injury class (K) based on min-max normalized GRF signals using a SVM as classifier.

4 CLASSIFICATION TASK: HC/A

4.1 Classifier: CNN
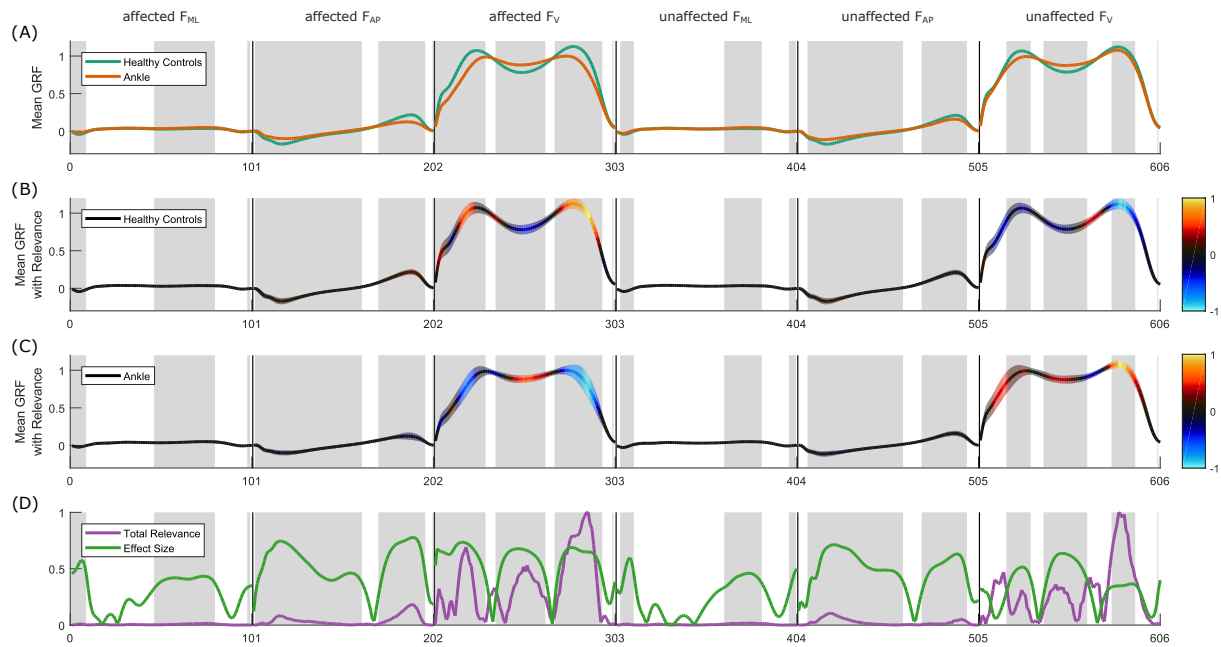
Supplementary Figure S 19. Result overview for the classification of healthy controls (HC) and ankle injury class (A) based on non-normalized GRF signals using a CNN as classifier.
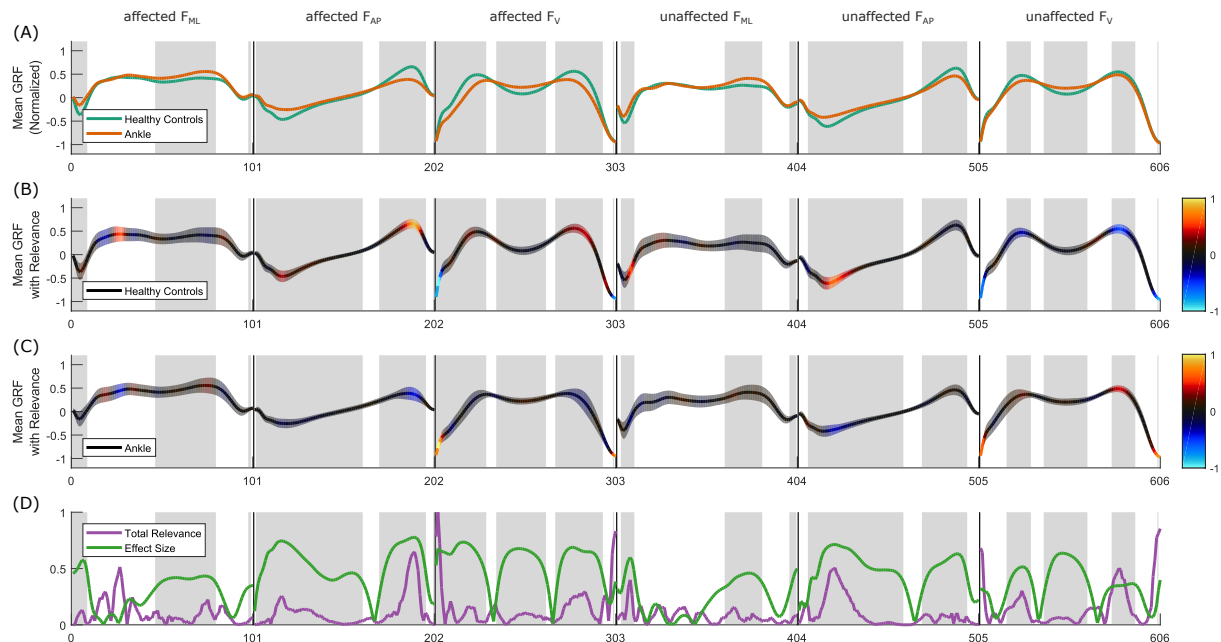

Supplementary Figure S 20. Result overview for the classification of healthy controls (HC) and ankle injury class (A) based on min-max normalized GRF signals using a CNN as classifier.

4.2 Classifier: MLP
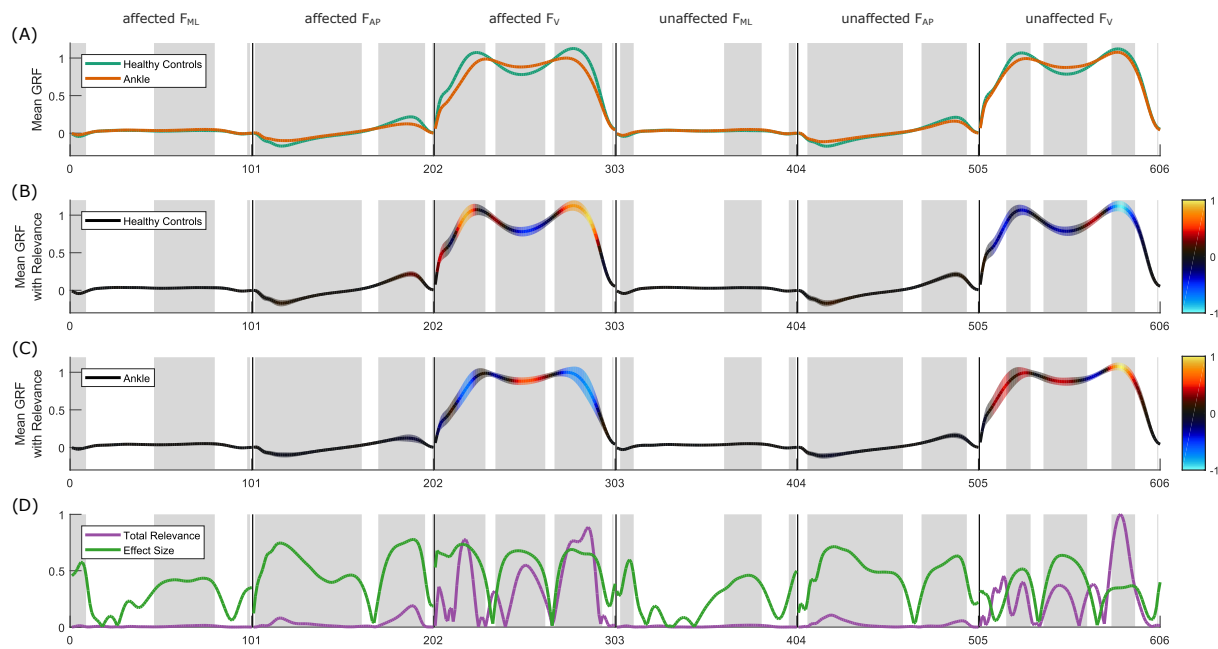
Supplementary Figure S 21. Result overview for the classification of healthy controls (HC) and ankle injury class (A) based on non-normalized GRF signals using a MLP as classifier.
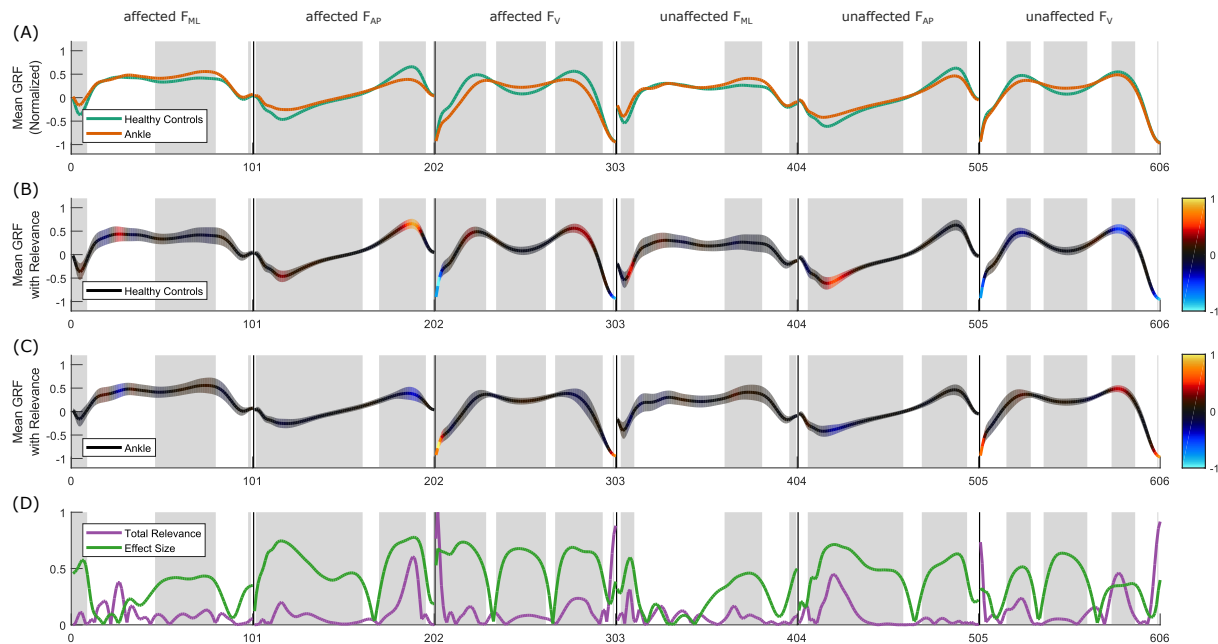

Supplementary Figure S 22. Result overview for the classification of healthy controls (HC) and ankle injury class (A) based on min-max normalized GRF signals using a MLP as classifier.

4.3   Classifier: SVM

Supplementary Figure S 23. Result overview for the classification of healthy controls (HC) and ankle injury class (A) based on non-normalized GRF signals using a SVM as classifier.

Supplementary Figure S 24. Result overview for the classification of healthy controls (HC) and ankle injury class (A) based on min-max normalized GRF signals using a SVM as classifier.